Precision study of supersymmetry at future linear e^+e^- colliders

Toshifumi Tsukamoto,[1] Keisuke Fujii,[1] Hitoshi Murayama,[2,3] Masahiro Yamaguchi,[3] and Yasuhiro Okada[1]

[1] *National Laboratory for High Energy Physics (KEK), Tsukuba 305, Japan*
[2] *Theoretical Physics Group, Lawrence Berkeley Laboratory, University of California, Berkeley, California 94720*
[3] *Department of Physics, Tohoku University, Sendai 980, Japan*
(Received 29 October 1993; revised manuscript received 27 September 1994)

We discuss a possible strategy for supersymmetry searches and studies at future linear e^+e^- colliders. We demonstrate their effectiveness by Monte Carlo analyses with full angular correlations under realistic experimental conditions including initial state radiation and beamstrahlung effects. The importance of precision measurements of supersymmetry parameters is emphasized. We demonstrate that the precision on mass measurements can be as good as 1% for leptonic and 3% for hadronic final states. A detailed study on the first superparticle alone gives us an upper bound on the next superparticle. We can also test the basic mass relations assumed in grand unified models or supergravity, such as the gaugino mass relations or the universal scalar mass assumption in a variety of ways. The polarized electron beam plays a critical role in this study.

PACS number(s): 14.80.Ly, 04.65.+e, 12.10.Dm, 13.10.+q

I. INTRODUCTION

The e^+e^- colliders have been playing complementary roles to the hadron colliders in high energy experiments. In general, e^+e^- colliders have reasonable signal rates in a clean environment with a definite center-of-mass energy, enabling us to perform precision measurements of particle masses, lifetimes, and various differential cross sections, while hadron colliders provide opportunities to quickly survey high energy frontier. Despite various beam-beam effects [1] including minijet productions [2], this cleanness persists up to TeV region [3–12]. In addition, future linear e^+e^- colliders such as the Japan Linear Collider (JLC) [5,6,8,10] will be equipped with a highly polarized electron beam using strained gallium arsenide or superlattice [13,14], with which a beam polarization of $P_{e^-} > 90\%$ is expected.

Experiments at the SLAC Linear Collider and CERN e^+e^- collider LEP demonstrated fully the above virtues of e^+e^- colliders. The precision measurements on the Z^0 resonance are now sensitive to one-loop quantum corrections, and have put a stringent constraint on the top quark mass [15]. Furthermore, the measured Weinberg angle $\sin^2\theta_W$ turned out to exclude the minimal model of the grand unified theory (GUT), but is consistent with its supersymmetric (SUSY) version. This observation raised revived interests in the SUSY models. SUSY predicts many new particles below TeV region. An e^+e^- collider is an ideal device to search for colorless superparticles which are believed to be relatively light compared to colored ones. Indeed, extensive studies have been made in Refs. [16–20], which demonstrated that the discovery of colorless superparticles is relatively easy in a clean e^+e^- environment [21].

In this paper, we focus on the precise determinations of supersymmetry parameters rather than search methods. The importance of the precision measurements of the parameters is twofold. (1) Once we discover at least

one superparticle, we can measure its properties and extract information on the SUSY parameters, which puts upper bounds on the next superparticles. We can thus set the next target center-of-mass energy to go up to. This property of the supersymmetric models permits us to successfully find new particles one after another. (2) The supersymmetric grand unification models (GUT) or the minimal supergravity scenario predict certain relations among the superparticle masses. We can test these relations and verify or exclude such models. For these purposes, the polarized electron beam plays an essential role [10,22]. It is noteworthy that the advantage of the polarized beam has not been fully appreciated in most of the previous analyses.

The analyses presented in this paper are guided by the following working hypothesis. Our input parameters are taken within the minimal supergravity scenario, but we reproduce them after Monte Carlo simulations with realistic detector and machine parameters, including initial state radiation and beamstrahlung effects, and demonstrate that the mass relations in the scenario can be tested experimentally. We focus on the strategy, not on the search limits, of the experiments at future linear e^+e^- colliders. Preliminary results from our analyses were already reported in Refs. [10,23,24]. Since then, we have examined new signal processes and refined our background studies with additional background processes which had been neglected in the previous reports. This paper summarizes our final results, including these new developments [25].

We first take a definite parameter set in the minimal supergravity scenario, assuming the universal scalar mass and GUT relation of the gaugino masses. Then we start with the lightest detectable superparticle ("first superparticle") which is a right-handed slepton in our choice of the SUSY parameters. By analyzing its properties in detail, we draw an upper bound on the next superparticle (chargino and second neutralino) using the GUT relation

of the gaugino masses, and simultaneously test the universal scalar mass assumption between the first and the second generations. Raising the center-of-mass energy to the next expected threshold, we study the chargino and again obtain a useful upper bound on the next to the next superparticle (left-handed slepton) by extracting the t channel sneutrino contribution. Its precise study again allows a stringent test on a consequence of GUT (the GUT relation of the gaugino masses). In this way, we can successively find many superparticles from the lightest to heavier ones, and also can make crucial tests on the GUT or supergravity assumptions.

The paper is organized as follows. In Sec. II we take a typical parameter set for which the "first superparticle" is a right-handed slepton. We perform Monte Carlo analyses along the line just described. In Sec. III we examine another case with a different parameter set, where the chargino is the "first superparticle." We also discuss possible difficulties we may encounter in the study of superparticles. Section IV concludes this paper. Appendix A summarizes the important mass relations within the GUT or supergravity models which are relevant to the analyses in this paper. A brief description of our Monte Carlo simulator is given in Appendix B, where the methods to incorporate the interference and angular correlations are also explained.

II. STRATEGY IN A LIGHT SLEPTON CASE

In this section, we describe our strategy for superparticle studies at a future linear e^+e^- collider for a sample case, where the right-handed slepton is the "first superparticle." We emphasize the importance of precision measurements of masses, total and differential cross sections; one can extract useful information on the next superparticle from such measurements. Moreover, we will be able to test various assumptions in SUSY-GUT or supergravity models.

The parameter set we take in our analyses is

$$
\begin{aligned}
m_0 &= 70 \text{ GeV}, \\
M_2 &= 250 \text{ GeV}, \\
\mu &= 400 \text{ GeV}, \\
\tan\beta &= 2,
\end{aligned}
\tag{1}
$$

which gives the following light superparticle mass spectrum:

$$
\begin{aligned}
\tilde{\chi}_1^0 &: 117.8 \text{ GeV}, \\
\tilde{l}_R &: 141.9 \text{ GeV}, \\
\tilde{\chi}_1^\pm &: 219.3 \text{ GeV}, \\
\tilde{\chi}_2^0 &: 221.5 \text{ GeV}, \\
\tilde{\nu}_L &: 227.2 \text{ GeV}, \\
\tilde{l}_L^\pm &: 235.5 \text{ GeV}.
\end{aligned}
\tag{2}
$$

Note that this parameter set also makes $\tilde{\chi}_1^0$ almost a pure B-ino because $M_1 \ll \mu$, and it is a good candidate for cold dark matter. The notation is explained in Appendix A.

A. Right-handed slepton

The production of right-handed sleptons occurs via the Feynman diagrams shown in Fig. 1. The three generations of the right-handed sleptons, $\tilde{e}_R$, $\tilde{\mu}_R$, and $\tilde{\tau}_R$, are usually assumed to be mass degenerate by the "universal scalar mass" assumption (see Appendix A). Among them, only the $\tilde{e}_R$-pair production process has the t channel diagram of neutralino exchange. Note that only the B-ino ($\tilde{B}$) component appears in this diagram, though the neutralino mass eigenstates may differ significantly from the pure B-ino state. $\tilde{\mu}_R$ and $\tilde{\tau}_R$ have only the s channel and γ- and Z^0-exchange diagrams, and the cross section and the angular distribution are determined solely by their gauge quantum numbers and spin. The production cross section of $\tilde{e}_R$ pairs is shown in Fig. 2(a), which shows that the process has a relatively large cross section of ~ 100 fb. The decay has a 100% branching fraction into $e\tilde{\chi}_1^0$, since it is the only kinematically available channel allowed by the R parity and the lepton number conservation, as long as the right-handed slepton is the "first superparticle." Therefore, the event signature to look for is an acoplanar lepton pair with large missing energy.

We generated signal and background events for the right-handed sleptons at $\sqrt{s} = 350$ GeV [26]. The event generation includes the effect of the initial state radiation as well as the beamstrahlung effects (for details, see Appendix B). The acoplanar lepton pair events were selected from the generated events by the following criteria: (1) e^+e^- or $\mu^+\mu^-$ with 5 GeV $< E_l < (\sqrt{s}-100$ GeV$)/2$, (2) 20 GeV $< E_{\text{vis}} < \sqrt{s}-100$ GeV, (3) $|m_{ll}-m_Z| > 10$ GeV, (4) $|\cos\theta_{l\pm}| < 0.9$, (5) $-Q\cos\theta_l < 0.75$ where Q is the charge of the lepton, and the polar angle is measured from the electron beam direction.

These cuts are similar to those employed in Refs. [16–19] except for cut 5. Our cuts are, however, somewhat weaker, resulting in larger detection efficiency, due mainly to the use of beam polarization which effectively removes the W^+W^- background. Cut 3 is to eliminate background events from the $e^+e^- \rightarrow Z^0Z^0$, $e^+e^-Z^0$, $\nu_e\bar{\nu}_eZ^0$ processes followed by $Z^0 \rightarrow l^+l^-$. Cuts 4 and
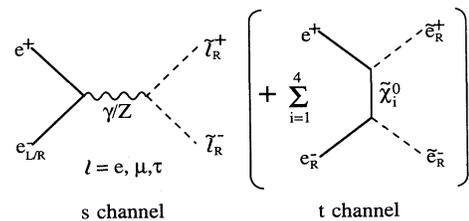

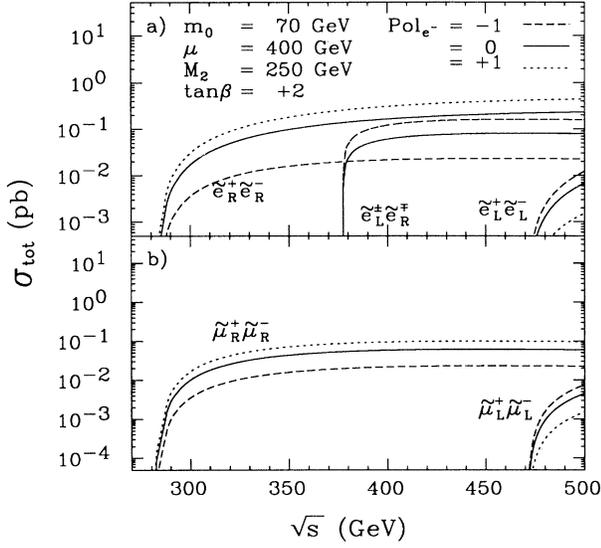FIG. 1. Feynman diagrams for the right-handed slepton-pair productions.

FIG. 2. Total cross sections for slepton productions: (a) $e^+e^- \to \tilde{e}_R^+\tilde{e}_R^-$, $e^+e^- \to \tilde{e}_L^\pm\tilde{e}_R^\mp$, and $e^+e^- \to \tilde{e}_L^+\tilde{e}_L^-$, (b) $e^+e^- \to \tilde{\mu}_R^+\tilde{\mu}_R^-$ and $e^+e^- \to \tilde{\mu}_L^+\tilde{\mu}_L^-$, where dashed, solid, and dotted lines correspond to electron beam polarizations of -1, 0, and $+1$, respectively. The cross sections were evaluated at the lowest order, without including initial state radiation or beam effects.

5, on the other hand, reduce the background from the W^+W^- and $e^\pm \overset{(-)}{\nu}_e W^\mp$ productions. The other background processes listed in Appendix B are found to be negligible. Figure 3(a) shows the acoplanarity distribution for the selected electron pairs from the $\tilde{e}_R$ decays (solid), together with the background from W^+W^- (dash) and $e^\pm \overset{(-)}{\nu}_e W^\mp$ (dot). There is a clear excess over the remaining background in the distribution. For the $\tilde{\mu}_R$ pairs, the signal-to-background ratio is lower than the $\tilde{e}_R$ case [see Fig. 3(b)] due to the lower cross section [see Fig. 2(b)]. One can, however, use a right-handed

electron beam, which enhances the signal and, at the same time, suppresses the background dramatically, as shown in Fig. 3(c) [27]. We assume a beam polarization of $P_{e^-} = 95\%$ hereafter, and impose an additional cut on the acoplanarity angle [28]: (6) $\theta_{\text{acop}} > 30°$. The resultant detection efficiencies are 45.0% for the $\tilde{e}_R$ pairs and 54.2% for the $\tilde{\mu}_R$ pairs with essentially no background.

The first analysis which should be performed on this clean event sample is to extract the masses of the sleptons and $\tilde{\chi}_1^0$ from the decay energy distribution of the final-state leptons [10]. Thanks to the simple two-body kinematics, the distribution should be flat with its two edges determined by the slepton and the lightest supersymmetric particle (LSP) masses. We shown in Fig. 4(a) the energy distribution of the final-state μ's for an integrated luminosity of 20 fb^{-1}. For the $\tilde{e}_R$ case, the measurement is easier since the cross section is higher. By making a two-parameter fit to the spectrum, we can determine their masses with a statistical error of $\pm 1\%$, as shown in Fig. 4(b).

It is also interesting to study the angular distribution of the sleptons. Once we know the slepton and the LSP masses, we can determine the slepton four-momenta from the final-state lepton momenta with a twofold ambiguity. Figure 5(a) plots the two solutions for the reconstructed $\tilde{\mu}_R$'s. Fortunately, the "wrong" solutions have a flat angular distribution, which can be easily subtracted to obtain Fig. 5(b). The figure clearly shows that the distribution behaves like $\sin^2\theta$, showing the particle has spin 0. The similar distributions for the selected $\tilde{e}_R$'s are shown in Figs. 6(a) and 6(b), where one can see a clear forward peak, indicating the t channel neutralino exchange. Since we already known the (LSP) mass, this distribution suggests that the LSP is dominated by the B-ino component. If the LSP is dominated by the Higgsino component, the distribution should look like that of the $\tilde{\mu}_R$-pair production.

One can also measure the polarization dependence of the cross sections. For the $\tilde{\mu}_R$ pair production, the cross sections for both beam polarizations are completely de-
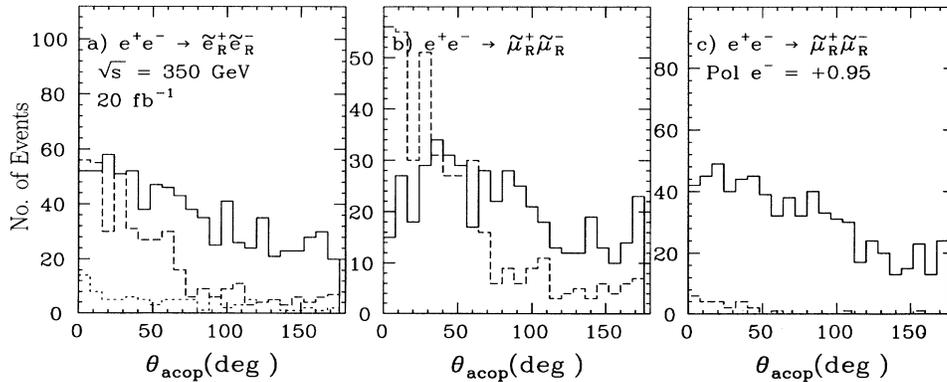

FIG. 3. Acoplanarity angle distributions for final-state leptons from right-handed slepton-pair productions (solid) at $\sqrt{s} = 350$ GeV with an integrated luminosity of 20 fb^{-1} after including the initial state radiation and the beamstrahlung effects: (a) $e^+e^- \to \tilde{e}_R^+\tilde{e}_R^-$ with $P_{e^-} = 0$, (b) $e^+e^- \to \tilde{\mu}_R^+\tilde{\mu}_R^-$ with $P_{e^-} = 0$, and (c) $e^+e^- \to \tilde{\mu}_R^+\tilde{\mu}_R^-$ with $P_{e^-} = +0.95$. The dashed lines indicate the W^+W^- background, while the dotted line represents that from the $e^\pm \overset{(-)}{\nu}_e W^\mp$ process.
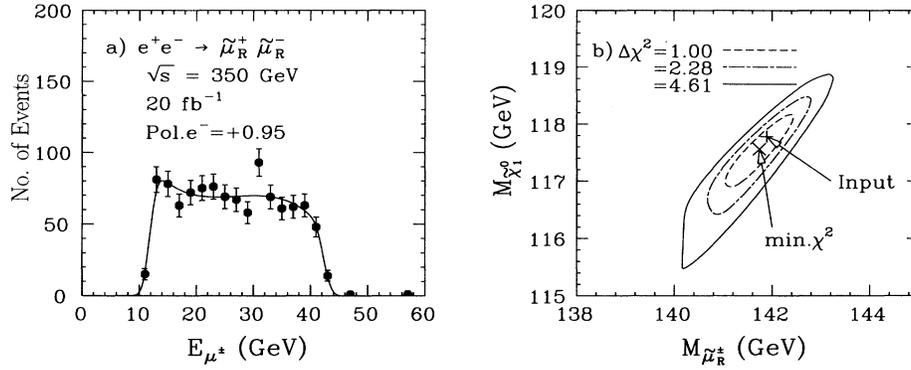
FIG. 4. (a) The energy distribution of final-state muons for $e^+e^- \to \tilde{\mu}_R^+\tilde{\mu}_R^-$ at $\sqrt{s} = 350$ GeV with an integrated luminosity of 20 fb^{-1} and an electron beam polarization of $P_{e^-} = +0.95$, after including the initial state radiation and the beamstrahlung effects. The smooth curve in the figure is the best-fit curve resulting from a two-parameter fit varying the $\tilde{\mu}_R$ and the $\tilde{\chi}_1^0$ masses. (b) Contours showing the errors on $m_{\tilde{\mu}_R}$ and $m_{\tilde{\chi}_1^0}$ expected for the two-parameter fit.

termined by the SU(2)$_L$ × U(1)$_Y$ quantum numbers. We can, thus, measure its hypercharge and third component of weak isospin from the cross sections alone. Then, we can confirm that it has indeed the same quantum numbers as those of μ_R and, together with the fact that it is spinless, they are superpartners. Note that the decay into $\mu + \tilde{\chi}_1^0$ alone does not tell us whether the parent scalar particle is either $\tilde{\mu}_R$ or $\tilde{\mu}_L$, even if we assume supersymmetry. For the $\tilde{e}_R$-pair production process, the t channel $\tilde{B}$ exchange diagram contributes only to the

production from the right-handed electron beam. If the beam is left-handed, therefore, only the s channel diagrams exist. Note that if $\tilde{\chi}_1^0$ is almost a pure Higgsino, then its t channel contribution is highly suppressed, and we expect $\sigma_R \simeq 4\sigma_L$, where the factor of 4 is simply the squared ratio of the hypercharges of e_L and e_R. If $\tilde{\chi}_1^0$ is almost a pure B-ino, then its t channel exchange dominates over the s channel diagram, and the cross section σ_R is much larger than $4\sigma_L$. Thus the cross sections alone give important information on the neutralino sector. Combined with the angular distribution, we obtain useful constraints on the $(M_2, \mu, \tan\beta)$ space, although we will not go into the analysis here.

The most important information we can extract from the slepton pair production is an upper bound on the lighter chargino ($\tilde{\chi}_1^\pm$) mass. One obtains the upper bound from the $\tilde{\chi}_1^0$ mass by assuming the GUT relation of the
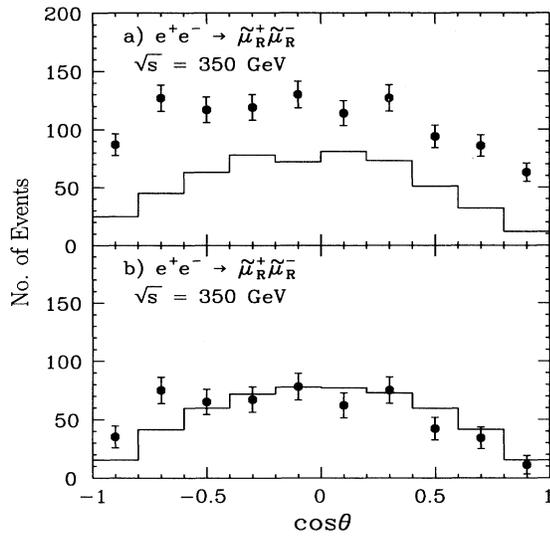
FIG. 5. The angular distribution of $\tilde{\mu}_R^-$'s in $e^+e^- \to \tilde{\mu}_R^+\tilde{\mu}_R^-$ reconstructed from final-state $\mu^\pm$ four-momenta, knowing the $\tilde{\mu}_R$ and $\tilde{\chi}_1^0$ masses and assuming no initial state radiation and no beamstrahlung: (a) with the two solutions unresolved and (b) with the background due to the wrong solutions subtracted. The Monte Carlo data were generated at $\sqrt{s} = 350$ GeV with an integrated luminosity of 20 fb^{-1} and $P_{e^-} = 0.95$ and plotted without acceptance correction. The histogram in (a) is the distribution of the right solutions, while that in (b) is the distribution of the original sample before selection cuts.
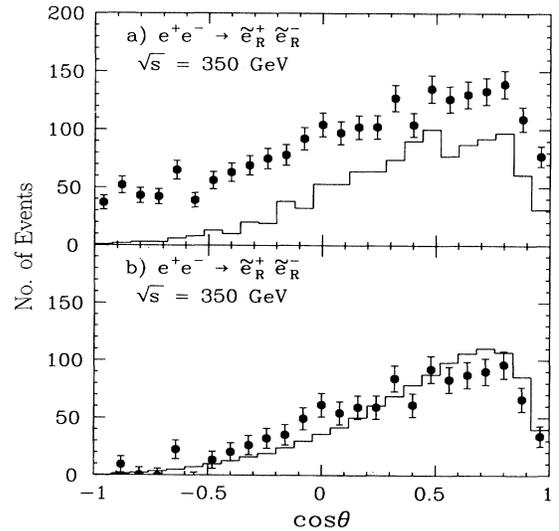
FIG. 6. Plots similar to Figs. 5(a) and 5(b) for $e^+e^- \to \tilde{e}_R^+\tilde{e}_R^-$.

gaugino masses and the minimal particle content in the neutralino and chargino sectors. Figure 7(a) shows this upper bound. One can intuitively understand this bound as follows. If $\tilde{\chi}_1^0$ is almost a pure Higgsino, then $\tilde{\chi}_1^\pm$ is also almost a pure Higgsino, and they should be nearly mass degenerate. If $\tilde{\chi}_1^0$ is almost a pure B-ino, then $\tilde{\chi}_1^\pm$ is almost a pure W-ino, which is $\frac{3}{5}\cot^2\theta_W = 2.0$ times as heavy as $\tilde{\chi}_1^0$. Since the reality is between these two extremes, $\tilde{\chi}_1^\pm$ should be lighter than $2.0 m_{\tilde{\chi}_1^0}$. A similar upper bound can be obtained for the second neutralino $\tilde{\chi}_2^0$ as well, as seen in Fig. 7(b). Therefore, the next target energy we should go up to is that for the associated $\tilde{\chi}_2^0\tilde{\chi}_1^0$ production or that for the pair production of $\tilde{\chi}_1^\pm$ or $\tilde{\chi}_2^0$. If they are not discovered within the predicted mass range, then the GUT relation is disproved, and the SUSY-GUT, at least that with the minimal particle content, faces a severe difficulty [29]. The upper bounds in our sample case are

$$m_{\tilde{\chi}_1^\pm}, m_{\tilde{\chi}_2^0} < 2.0 m_{\tilde{\chi}_1^0} \simeq 240 \text{ GeV}. \tag{3}$$

The slepton mass determinations are in themselves very important, since they allow us an essential test on the minimal supergravity scenario, whether or not the scalar masses are generation independent. Figure 8 shows the test on the generation independence of the measured masses of $\tilde{e}_R$ and $\tilde{\mu}_R$.

Tables I and II summarize the observable quantities for the right-handed slepton production and their implications, respectively.

B. Neutralino associated production

Since we now have the upper bound on the mass of $\tilde{\chi}_2^0$, we can set the energy to study the $\tilde{\chi}_1^0\tilde{\chi}_2^0$ associate production process at $\sqrt{s} = 400$ GeV. Unfortunately, the cross section for this process is rather low, ~ 10 fb for our parameter set, and there is the large "background" from the right-handed slepton pair production, although the background from the W-pair production can be effectively suppressed by using the right-handed electron beam at the cost of some loss of the signal cross section [30]. Therefore, this process can be used only to check the existence $\tilde{\chi}_2^0$ predicted from the LSP mass and the GUT relation.

In our parameter choice, the dominant decay mode is $\tilde{\chi}_2^0 \to \tilde{l}_R^\pm l^\mp$ and its charge conjugate, which leads to a final state consisting of an acoplanar lepton pair with large missing energy. Such events can be selected with the same criteria as with the right-handed slepton pair. The use of acoplanar $\mu^+\mu^-$ final states is more advantageous than that of acoplanar e^+e^- final states, since the latter suffers from $\tilde{e}_L^\pm \tilde{e}_R^\mp$ "background," the channel which is already open at this center-of-mass energy for our parameter set [31]. Figure 9(a) is the scatter plot of the muon energies for an integrated luminosity of 20 fb^{-1} and a beam polarization of $P_{e^-} = 95\%$. The background from the W^+W^- production is very small, thanks to the beam polarization [see Fig. 9(b)]. The "background" from the right-handed slepton pair production has much lower lepton energies, as shown in Fig. 9(c), while the leptons from the $\tilde{\chi}_2^0$ decays have higher energies. After the cuts indicated in the figures, the number of signal events is 20, while that from the W^+W^- background is 10. The statistical significance is about 4σ. Therefore, one can verify the existence of $\tilde{\chi}_2^0$, although the statistics are too low for precise studies.

The $\tilde{\chi}_2^0$ mass can be measured, however, using its pair production: although the $\tilde{\chi}_2^0$ mass is similar to that of $\tilde{\chi}_1^\pm$ for our parameter set, we can easily separate $\tilde{\chi}_2^0$-pair events from $\tilde{\chi}_1^\pm$-pair events by using the four-lepton final state from a $\tilde{\chi}_2^0$ pair, which is essentially background free.

C. Chargino pair production

Considering the upper bound on the mass of the lighter chargino from the right-handed slepton studies, we fix the center-of-mass energy at $\sqrt{s} = 500$ GeV. If we do not discover the chargino below the upper bound, then it will disprove the SUSY-GUT, at least that with the minimal particle content [29]. If we discover it, then we can measure the parameters of the neutralino or chargino sector precisely. What is most exciting here is that we can test whether or not the GUT relation on the gaugino masses holds.

For the parameters in our sample case, the chargino decays mainly into a two-body final state: $\tilde{\chi}_1^\pm \to \tilde{\chi}_1^0 W^\pm$. The event signature is thus an acoplanar W pair with large missing energy. The W bosons in the final state can be easily reconstructed by the jet invariant mass
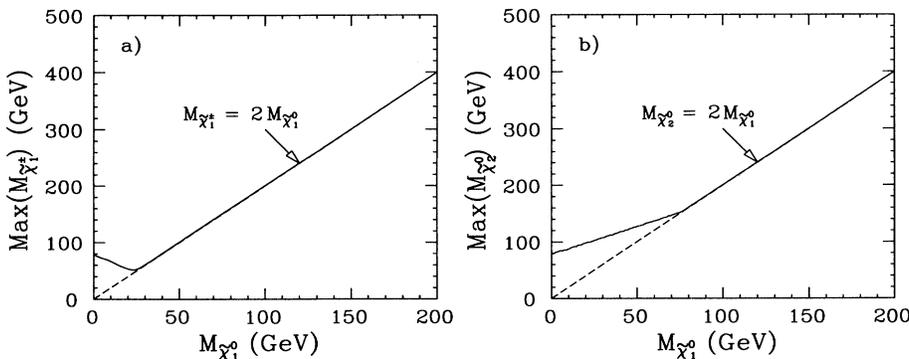

FIG. 7. The upper limits on (a) $m_{\tilde{\chi}_1^\pm}$ and (b) $m_{\tilde{\chi}_2^0}$ as functions of $m_{\tilde{\chi}_1^0}$ assuming the GUT relation on the gaugino masses. The limits become $2.0 \times m_{\tilde{\chi}_1^0}$ in the high-$m_{\tilde{\chi}_1^0}$ region, as indicated by dashed lines.
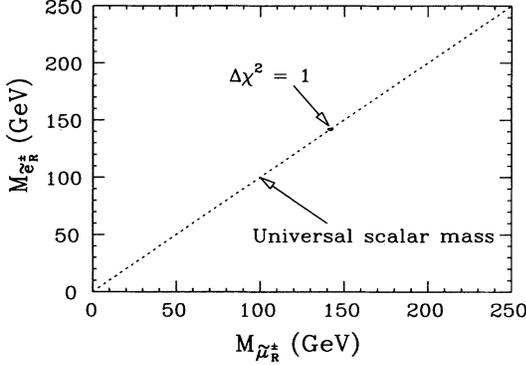
FIG. 8. The $\Delta\chi^2 = 1$ contour in the $m_{\tilde{\mu}_R}$-$m_{\tilde{e}_R}$ plane obtained from fits to the final-state lepton energy distributions for the $\tilde{\mu}_R$- and $\tilde{e}_R$-pair productions. The dotted line corresponds to the universal scalar mass hypothesis.

TABLE I. The observables in the right-handed slepton pair production.

$m_{\tilde{e}_R}, m_{\tilde{\chi}_1^0}, m_{\tilde{\mu}_R}, \sigma_L(\tilde{e}_R), \sigma_R(\tilde{e}_R)$,
$\sigma_L(\tilde{\mu}_R), \sigma_R(\tilde{\mu}_R)$, angular distributions

method [32]. We did not discuss the two-body decay case in Refs. [10,24], since it was expected, in general, to be easier than the three-body decay case in Sec. III A. In our parameter choice, however, t channel sneutrino exchange reduces the total cross section dramatically [16] and make its study more difficult than expected. We will demonstrate here that mass measurement at 5% level is still possible.

We use the following selection criteria to select acoplanar W pair events in the four-jet mode: (1) the number of charged tracks > 20, (2) 20 GeV < E_{vis} < $\sqrt{s} - 100$ GeV, (3) there is no lepton (e or μ) with E_l > 25 GeV, (4) there exists a y_{cut} greater than 5×10^{-3} resulting in four jets, two of which satisfy $|\cos\theta_j|$ < 0.8 and the remaining two satisfy $|\cos\theta_j|$ < 0.95, (5) the four jets can be grouped into two pairs of jets consistent with the W mass, $m_W - 10$ GeV < m_{jj} < $m_W + 20$ GeV, (6) each of the two W candidates has a production angle $|\cos\theta_W|$ < 0.9, (7) the missing mass is inconsistent with the $W^+W^-Z^0(\to \nu\bar{\nu})$ hypothesis, $m_{\text{missing}} \leq 70$ GeV or $m_{\text{missing}} \geq 120$ GeV, and (8) θ_{acop} > 30°.

The cuts employed here are similar to those employed in Ref. [16]. The detection efficiency after these cuts was estimated to be 10.8%, including the branching fraction into the four-jet final states. Figure 10 shows the acoplanarity angle distribution for the remaining events after all but the acoplanarity cut, when an integrated luminosity of 50 fb^{-1} is accumulated. One can clearly see an excess over the background from the W^+W^- (dash), the $e^+e^-W^+W^-$ (dot), and the sum of the $e^{\pm} \overset{(-)}{\nu}_e W^{\mp}Z^0$, $W^+W^-Z^0$, and $\nu_e\bar{\nu}_eW^+W^-$ (dot-dash) productions. The selection cuts effectively remove, to a negligible level, the background from the other processes

such as $e^+e^- \to Z^0Z^0$, $Z^0Z^0Z^0$, and $\nu_e\bar{\nu}_eZ^0Z^0$. The distribution of the W energies is flat, thanks to the simple two-body kinematics. Monte Carlo data including the detector and the beam effects suggest this simple kinematics as shown in Fig. 11(a). A fit to the event sample gives the masses of $\tilde{\chi}_1^{\pm}$ and $\tilde{\chi}_1^0$ [see Fig. 11(b)]. Here we can make a cross check on the mass of $\tilde{\chi}_1^0$ by comparing it with that measured for the slepton production. For an integrated luminosity of 50 fb^{-1}, the error on the $\tilde{\chi}_1^{\pm}$ mass is expected to be ±10 GeV. This error reduces to ±5 GeV when combined with the $m_{\tilde{\chi}_1^0}$ measured for the right-handed slepton decays [33].

One can also study the angular distribution of $\tilde{\chi}_1^{\pm}$'s. Similarly to the case of the right-handed slepton-pair production, one can determine the four-momenta of the charginos up to a twofold ambiguity, once their masses are known. Figure 12(a) plots the angular distribution with the twofold ambiguity unresolved. The "wrong" solutions again give an almost flat distribution, which can be subtracted to reproduce the real angular distribution as shown in Fig. 12(b) [34]. The event excess in the forward region suggests that there is some diagram with t channel particle exchange. The only particle exchanged in the t channel here is the electron sneutrino $\tilde{\nu}_{e_L}$.

An important analysis can be made with the beam polarization. Recall that the charged W-ino $\tilde{W}^{\pm}$ is not produced from the right-handed beam just like the W boson [suppressed by a factor of $(m_Z^2/s)^2 < 10^{-3}$ in our case], while the charged Higgsino $\tilde{H}^{\pm}$ has roughly the same cross sections (up to a factor of ~ 4) for the left- and right-handed electron beams. Thus the cross section for the right-handed electron beam "measures" the Higgsino component of the chargino. We have four independent observables concerning the neutralino or chargino sector:

$$m_{\tilde{\chi}_1^0}, \quad m_{\tilde{\chi}_1^{\pm}}, \quad \sigma_R(\tilde{e}_R), \quad \sigma_R(\tilde{\chi}_1^{\pm}). \qquad (4)$$

The masses are directly related to the neutralino or chargino mass matrix. The cross section $\sigma_R(\tilde{e}_R)$ has the contribution from the t channel neutralino exchange. $\sigma_R(\tilde{\chi}_1^{\pm})$ carries the information on the Higgsino component in $\tilde{\chi}_1^{\pm}$. Then we can perform a global fit, varying the parameters

$$M_1, \quad M_2, \quad \mu, \quad \tan\beta, \qquad (5)$$

TABLE II. The physics implications of the observables in the right-handed slepton pair production.

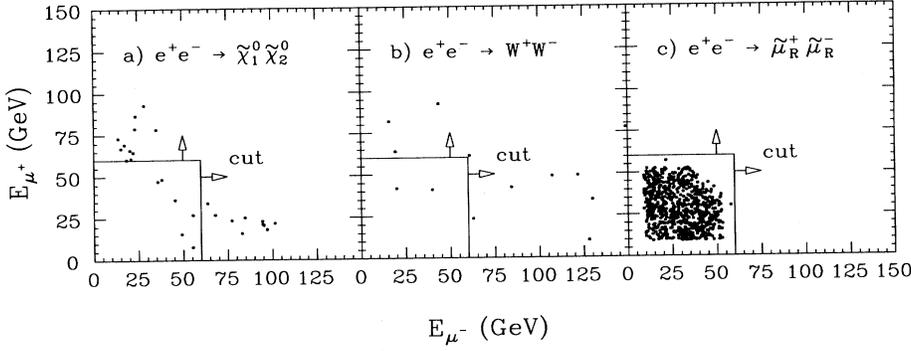|	
Upper bound on lighter chargino mass	$m_{\tilde{\chi}_1^0}$
Test of universal scalar mass	$m_{\tilde{e}_R}, m_{\tilde{\mu}_R}$
Check of the slepton quantum numbers	$\sigma_L(\tilde{e}_R), \sigma_L(\tilde{\mu}_R), \sigma_R(\tilde{\mu}_R)$
Constraints on neutralino parameters	$m_{\tilde{e}_R}, \sigma_R(\tilde{e}_R), m_{\tilde{\chi}_1^0}, d\sigma_R(\tilde{e}_R)/d\cos\theta$

FIG. 9. Scatter plots of $\mu^{\pm}$ energies at $\sqrt{s}$ = 400 GeV for (a) $e^+e^- \rightarrow \tilde{\chi}_1^0\tilde{\chi}_2^0$, (b) $e^+e^- \rightarrow W^+W^-$, and (c) $e^+e^- \rightarrow \tilde{\mu}_R^+\tilde{\mu}_R^-$, assuming an integrated luminosity of 20 fb^{-1} and an electron beam polarization of P_{e^-} = +0.95, and including the initial state radiation and the beamstrahlung effects. The square boxes in the figures indicate the locations of cuts to select $\tilde{\chi}_1^0\tilde{\chi}_2^0$ events.

from which we can test the GUT relation $M_1/M_2 = \frac{5}{3}\tan^2\theta_W$. Figure 13(a) shows the resultant contours in the M_1 and M_2 plane corresponding to $\Delta\chi^2 = 1$ (dash), 2.28 (dot-dash), and 4.61 (solid) [35]. In this way, we can test the SUSY-GUT prediction at the $\sim 5\%$ level. Figures 13(b) and 13(c) are, on the other hand, the corresponding contours in the (M_2, μ) and $(M_2, \tan\beta)$ planes, respectively. It is remarkable that we could obtain an upper bound on μ even though the "observed" chargino and neutralino are almost pure gauginos.

In our sample case, one can understand the sensitivity to various parameters in the following way. By expanding the four quantities we used in the global fit in powers of m_Z/μ or m_W/μ, we obtain

$$m_{\tilde{\chi}_1^0} \simeq M_1 - \frac{m_Z^2\sin^2\theta_W}{\mu^2 - M_1^2}(M_1 + \mu\sin2\beta), \qquad (6)$$

$$m_{\tilde{\chi}_1^\pm} \simeq M_2 - \frac{m_W^2}{\mu^2 - M_2^2}(M_2 + \mu\sin2\beta), \qquad (7)$$

$$\sigma_R(\tilde{e}_R) \simeq \sigma_R^0(\tilde{e}_R)\left(1 - 2\frac{m_Z^2}{\mu^2}\sin^2\theta_W\right), \qquad (8)$$

$$\sigma_R(\tilde{\chi}_1^\pm) \simeq \sigma_{pt}\frac{\beta}{16}\left(\frac{\sqrt{2}m_W}{\mu^2 - M_2^2}\right)^4$$
$$\times(\mu^2 + M_2^2 + 2\mu M_2\sin2\beta)^2, \qquad (9)$$

where σ_{pt} is the QED $e^+e^- \rightarrow \mu^+\mu^-$ cross section evaluated with the running coupling $\alpha = 1/128$. As stressed earlier, the cross sections alone suggest our LSP is B-ino rich and our $\tilde{\chi}_1^\pm$ is Wino rich, which implies a lower bound on μ: $\mu > 280$ GeV at a 1σ level. The mixing in the neutralino sector reduces the cross section $\sigma_R(\tilde{e}_R)$ from $\sigma_R^0(\tilde{e}_R)$ evaluated with a pure B-ino LSP. The amount of the reduction decreases as μ goes up and roughly corresponds to a 1σ statistical significance for our parameter set. On the other hand, $\sigma_R(\tilde{X}_1^\pm)$ is almost vanishing (0.3 fb) for a pure W-ino, while, for our parameter set, it results in a 1σ excess of events over the background from the "wrong" polarization of 5%: 5 events from right-handed and 10 events from left-handed electrons. Both of

these two cross section measurements thus require some Higgsino components in $\tilde{\chi}_1^0$ and $\tilde{\chi}_1^\pm$ and combine to put a 1σ level upper bound on μ of 530 GeV [36]. On the other hand, almost no information on $\tan\beta$ can be extracted from the cross sections, since one can always reproduce $\sigma_R(\tilde{\chi}_1^\pm)$ by adjusting μ within the measurement error for any $\tan\beta$. Nevertheless, since both $\sin2\beta$ and μ are bounded and μ is large, the LSP and the chargino masses mainly determine M_1 and M_2: the errors on M_1 and M_2 are thus dominated by the errors on $m_{\tilde{\chi}_1^0}$ and $m_{\tilde{\chi}_1^\pm}$ [37].

Another important piece of information can be obtained from the cross section for the left-handed electron beam, which was not used in the fit. The left-handed electron beam allows a t channel exchange of $\tilde{\nu}_e$, which interferes destructively with the s channel gauge boson exchange diagrams. Since we already know the composition of the chargino from the previous analysis, the only unknown parameter here is the mass of $\tilde{\nu}_e$. We show in Fig. 14 the dependence of the cross section on $m_{\tilde{\nu}_e}$ for P_{e^-} = 0. In our choice of parameters, the cross section is sensitive to $m_{\tilde{\nu}_e}$, because the chargino state is almost a W-ino and the sneutrino is not too heavy, and hence we
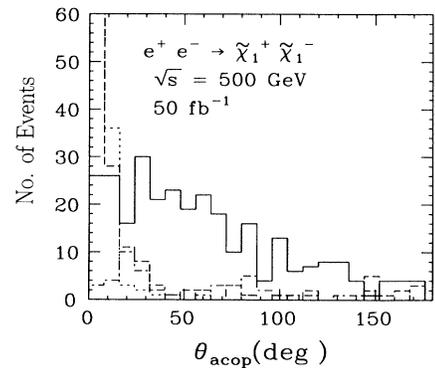

FIG. 10. Acoplanarity angle distributions of W pairs from $e^+e^- \rightarrow \tilde{\chi}_1^+\tilde{\chi}_1^-$ (solid), $e^+e^- \rightarrow W^+W^-$ (dash), $e^+e^- \rightarrow W^+W^-$ (dot), and the other background processes: $e^+e^- \rightarrow e^{\pm} \overset{(-)}{\nu}_e W^{\mp}Z^0$, $W^+W^-Z^0(\rightarrow \nu\bar{\nu})$, and $\nu_e\bar{\nu}_eW^+W^-$ (dot-dash) at $\sqrt{s}$ = 500 GeV with an integrated luminosity of 50 fb^{-1}, after including the initial state radiation and the beamstrahlung effects.
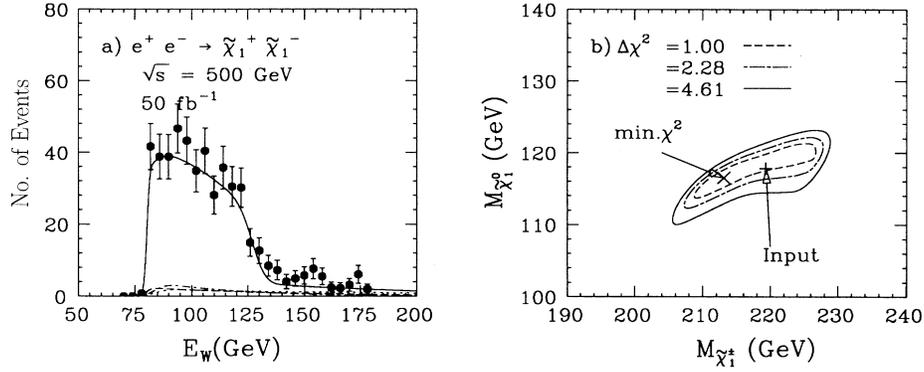
FIG. 11. (a) The energy distribution of W candidates in the final sample defined in the text. The Monte Carlo events include both the signal $(e^+e^- \to \tilde{\chi}_1^+ \tilde{\chi}_1^-)$ and the background generated at $\sqrt{s} = 500$ GeV with an integrated luminosity of 50 fb^{-1}, including the initial state radiation and the beamstrahlung effects. The dashed, the dot-dashed, and the dotted curves show the expected shapes of the backgrounds from the W^+W^-, the $e^{\pm} \overset{(-)}{\nu}_e W^{\mp} Z^0$, and the other processes $(W^+W^-Z^0, e^+e^-W^+W^-, \nu_e\bar{\nu}_e W^+W^-)$, respectively, while the solid line is the best-fit curve obtained from a two-parameter $(m_{\tilde{\chi}_1^0}$ and $m_{\tilde{\chi}_1^\pm})$ fit to the energy distribution. The fit takes into account the shapes of the background distributions. (b) The contours resulting from the two-parameter fit.

can measure the mass of $\tilde{\nu}_e$ fairly well. The measured $\tilde{\nu}_e$ mass sets an upper bound on the mass of the left-handed slepton $\tilde{e}_L$ (see Appendix A) [38]:

$$m_{\tilde{e}_L}^2 \leq m_{\tilde{\nu}_e}^2 + 0.77 m_Z^2. \qquad (10)$$

Thus we have again the next target energy to hunt the next superparticle.

Tables III and IV summarize the observables and their implications for the chargino production, respectively.

D. Left-handed slepton

The production of the left-handed slepton occurs first in the associate production process, $e^+e^- \to \tilde{e}_L^{\pm} \tilde{e}_R^{\mp}$. This requires a lower center-of-mass energy than the pair production which we discussed before in Ref. [10]. The Feynman diagram is shown in Fig. 15. Here, only the t channel $\tilde{B}$-exchange contributes, and s channel gauge boson exchange diagrams are absent due to the "chirality" of the scalar particles in the supersymmetric gauge theory. The cross section is reasonable if $\tilde{B}$ is relatively light. Since we already know the chargino or neutralino parameters by this moment, we can make definite predictions of the cross section and the angular distribution with the only one unknown parameter, $m_{\tilde{e}_L}$.

Figure 2(a) shows the cross section for $e^+e^- \to \tilde{e}_L^{\pm} \tilde{e}_R^{\mp}$. Notice that the cross section increases as β in the threshold region, contrary to that of the $\tilde{l}_R$- or $\tilde{l}_L$-pair production, which rises as β^3. This is due to the S-wave production of the sleptons, which demonstrates the conservation of chirality that left- (right-) handed selectrons couple only to left- (right-) handed electrons. Since this chiral selection rule is essential to ensuring the absence of quadratic divergences in scalar masses in supersymmetric theories, its experimental test is interesting.

The decay of the left-handed slepton may be a little complicated. Figure 16 gives the branching fractions into the two-body final state $\tilde{e}_L \to e\tilde{\chi}_1^0$ for various parameters. As the scalar mass becomes heavier, the left-handed slepton tends to decay into multibody final states. Nevertheless, there is still more than $\sim 10\%$ branching fractions into the two-body final state. For our parameter set, the two-body decay mode is actually dominant.

We set the center-of-mass energy at $\sqrt{s} = 400$ GeV [39] and employ the same selection criteria used for the right-handed slepton-pair production, which result in an overall detection efficiency of 44.5%. Here again, the W-pair production, which would be the largest background, can be effectively suppressed by the use of the right-handed electron beam, leaving the $\tilde{e}_R$-pair production as the dominant background. Notice, however, that the charge of the produced selectrons is uniquely fixed for a 100%-polarized beam: $e^+e_R^- \to \tilde{e}_L^+\tilde{e}_R^-$. Figure 17 is the scatter plot of the electron and positron energies for an integrated luminosity of 20 fb^{-1} and a realistic polarization $P_{e^-} = 95\%$. The figure shows that the events from the $\tilde{e}_R$ pair and the associate productions are clearly separated [40]. We perform a two-parameter fit to the energy distribution of the positrons to determine the left-handed slepton mass [see Figs. 18(a) and 18(b)]. The expected error on the $\tilde{e}_L$ mass is ± 2.5 GeV for an integrated luminosity of 20 fb^{-1}. A consistency check between the measured $m_{\tilde{\chi}_1^0}$ with those measured for the $\tilde{l}_R$- and $\tilde{\chi}_1^{\pm}$-pair productions can be made, and the sensitivity to $m_{\tilde{e}_L}$ can be further improved by including in the fit the $m_{\tilde{\chi}_1^0}$'s measured earlier.

The comparison of the masses of $\tilde{e}_R$ and $\tilde{e}_L$ is of our great interest. The difference $m_{\tilde{e}_L}^2 - m_{\tilde{e}_R}^2$ directly reflects the mass difference of the $\mathbf{5^*}$ and the $\mathbf{10}$ representations of the SU(5) GUT, while the universal scalar mass assumption in the minimal supergravity predicts that they have the same mass. Figure 19 compares the
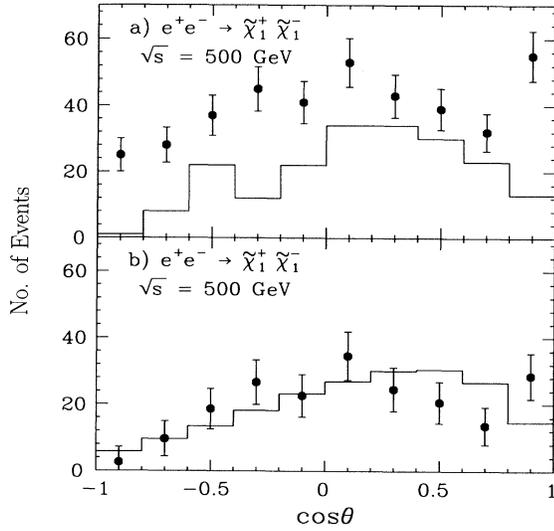
FIG. 12. (a) An example of the reconstructed production angle distribution (data points) compared with the generated angle distribution of the selected sample (histogram). The Monte Carlo events were generated at $\sqrt{s} = 500$ GeV and correspond to an integrated luminosity of 50 fb^{-1}. We have assumed a 100% charge ID efficiency for W's here. The production angles were reconstructed from the four-jet final states, knowing the W, the chargino, and the LSP masses and assuming no initial state radiation and no beamstrahlung. The two solutions were plotted in the same figure. (b) Same as (a) but after the subtraction of the background due to wrong solutions. The histogram is the scaled generated angle distribution for the initial sample before selection cuts, while the data points are the reconstructed without acceptance correction.

so-determined values with the prediction.

After measuring the $\tilde{e}_L$ mass, the generation universality assumed in the supergravity scenario tells us that $\tilde{\mu}_L$ and $\tilde{\tau}_L$ are mass degenerate with $\tilde{e}_L$. Then we can go up to the threshold of their pair productions.

Tables V and VI summarize the observables and their implications for the slepton associate production, respectively.

E. Heavier superparticles

Instead of presenting detailed analyses on the heavier superparticles, whose masses are presumably predicted by this point of the SUSY studies, we briefly discuss some features of their searches below.

The second neutralino $\tilde{\chi}_2^0$ decays via $\tilde{l}_L$ exchange dominantly into $l^+l^-\tilde{\chi}_1^0$ or $\nu_l\bar{\nu}_l\tilde{\chi}_1^0$ in our parameter set. Therefore, $\tilde{\chi}_2^0$-pair production has a very clean signal of acoplanar four-leptons, which is essentially background-free. Though the threshold of $\tilde{\chi}_2^0$-pair production is almost degenerate with that of $\tilde{\chi}_1^{\pm}$-pair production, there is no problem with their identification because of their different signatures. This is a virtue of an e^+e^- machine that allows us to use both hadronic and leptonic modes. Com-

bined with studies on the lighter chargino discussed in the preceding section, the studies on the second neutralino overconstrain the neutralino or chargino mass matrices. Although the $\tilde{l}_L$-pair production has a higher rate by a factor of 4 for the left-handed than the right-handed electron beam, it is better to employ the right-handed electron beam in order to avoid the W-pair background. The $\tilde{e}_L$-pair production has t channel exchange diagrams of both $\tilde{B}$ and $\tilde{W}$ components of neutralinos, and its cross section and angular distribution are worth studying.
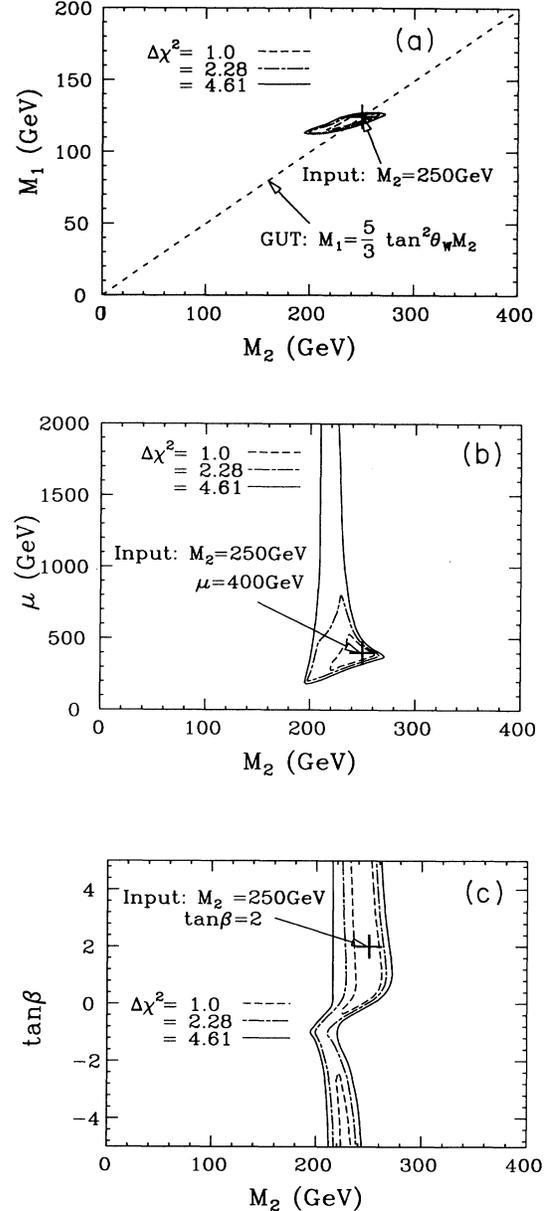

FIG. 13. The $\Delta\chi^2 = 1$ (dash), 2.28 (dot-dash), and 4.61 (solid) contours in (a) M_2-M_1, (b) M_2-μ, and (c) M_2-tanβ planes, which were obtained from the global fit explained in the text. The dotted line in (a) indicates the GUT prediction: $M_1 = \frac{5}{3}\tan^2\theta_W M_2$.
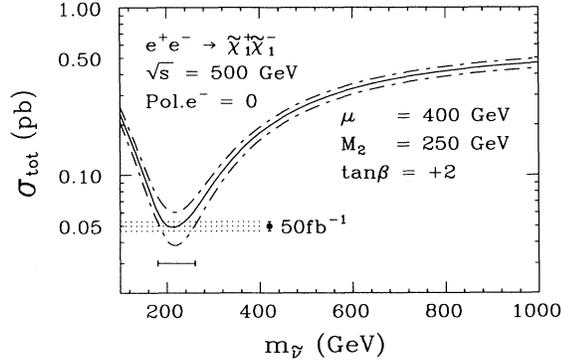
FIG. 14. The total cross section for $e^+e^- \to \tilde{\chi}_1^+\tilde{\chi}_1^-$ at $\sqrt{s} = 500$ GeV as a function of the mass of electron sneutrino. The cross section was evaluated at the lowest order without including initial state radiation nor beam effects for an unpolarized electron beam $P_{e^-} = 0$. The dot-dashed curves represent the $\pm 1\sigma$ bounds from the global fit explained in the text.
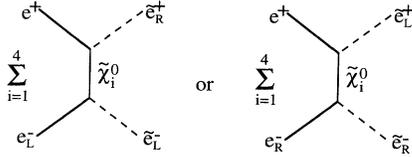

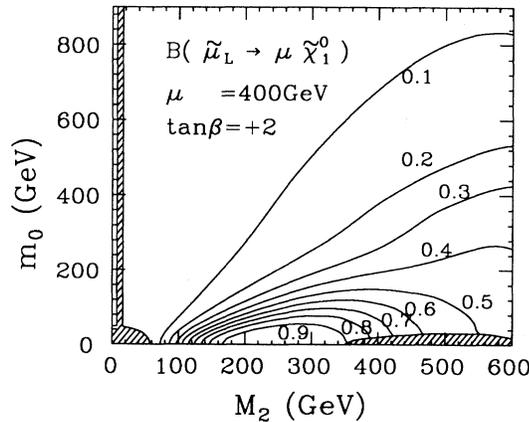FIG. 15. The Feynman diagram for $e^+e^- \to \tilde{e}_L^\pm \tilde{e}_R^\mp$.

FIG. 16. The branching fraction of $\tilde{e}_L^\pm$ into $e^\pm\tilde{\chi}_1^0$ in the plane of M_2 and m_0. The shaded regions correspond to the case where the LSP is not the lightest neutralino.
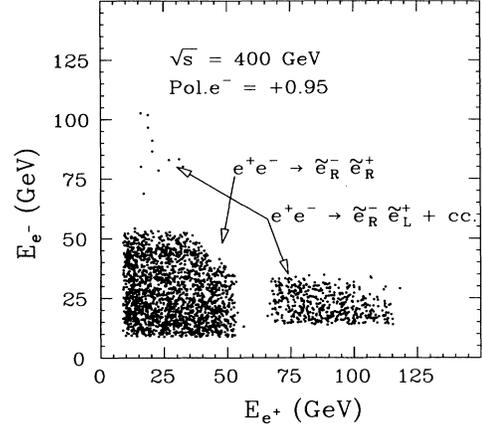

FIG. 17. The scatter of plot of $e^\pm$ energies at $\sqrt{s} = 400$ GeV with an integrated luminosity of 20 fb^{-1} and an electron beam polarization of $P_{e^-} = +0.95$ for $e^+e^- \to \tilde{e}_L^\pm\tilde{e}_R^\mp$ and $e^+e^- \to \tilde{e}_R^+\tilde{e}_R^-$, including the initial state radiation and the beamstrahlung effects.

After studying the right-handed sleptons, the lighter chargino, the second neutralino, and the left-handed sleptons, we will probably reach the thresholds of other heavy superparticles as well, like the heavier chargino, and the heavier neutralinos which may decay into charged particles. After crossing these thresholds, the experiment becomes quite messy. We know, however, the basic parameters of the chargino or neutralino sector already, and we can still make a consistency check of the measured parameters, comparing the observed events with the Monte Carlo predictions. The resulting events are highly dependent on the precise values of the parameters, and we believe it is premature to perform a Monte Carlo analysis in this paper.

The most important physics goal above the thresholds of the heavier superparticles is to test the overall consistency of the events with the supersymmetric Lagrangian. Since the supersymmetric Lagrangian is tightly constrained, the overall consistency is a measure whether the interactions are indeed described by a supersymmetric theory or not [41].

III. DISCUSSIONS ON OTHER CASES

In the preceding section, we have extensively studied the SUSY search and study strategy for a particular choice of SUSY parameters, where we demonstrated how the precise studies, possible only at an e^+e^- collider, give useful information on the next superparticles, with which we can go up to higher energies, step by step, with some confidence. In this section, we discuss how the situation changes, when we take different sets of parameters.

TABLE III. The observables in the chargino pair production.

$m_{\tilde{\chi}_1^\pm}, \sigma_L(\tilde{\chi}_1^\pm), \sigma_R(\tilde{\chi}_1^\pm)$, angular distributions

TABLE IV. The physics implications of the observables in the chargino pair production.

Higgsino content of $\tilde{\chi}_1^\pm$	$m_{\tilde{\chi}_1^\pm}, \sigma_R(\tilde{\chi}_1^\pm)$, angular distribution
Test on GUT relation of gaugino masses	$m_{\tilde{\chi}_1^\pm}, \sigma_R(\tilde{\chi}_1^\pm)$, angular distribution, $\sigma_R(\tilde{e}_R), m_{\tilde{\chi}_1^0}$
Sneutrino mass	$\sigma_R(\tilde{\chi}_1^\pm)$, angular distribution

A. Chargino lighter than slepton

It is also possible that the chargino is lighter than the right-handed sleptons. In this case, we will discover the chargino first. We improve our previous analyses to include more background processes here, since we had only W^+W^- in Ref. [10] or W^+W^-, $W^+W^-Z^0$, and $e^\pm \overset{(-)}{\nu}_e W^\mp$ in Ref. [24].

The Feynman diagrams for the chargino-pair production are shown in Fig. 20. Note that there is a t channel exchange diagram of electron-sneutrino $\tilde{\nu}_e$, which contributes to the process only if the electron beam is left handed. The cross section for the right-handed electron beam is determined solely by the chargino parameters.

In a large fraction of the chargino parameter space (M_2, μ), the lightest chargino decays into the two-body final state: $\tilde{\chi}_1^\pm \to \tilde{\chi}_1^0 W^\pm$. Since the daughter W's can be easily reconstructed by the jet invariant mass method, we can study the acoplanarity distribution of the final-state W's, as we did in the preceding section. If the chargino decays into a three-body final state, however, the situation will be somewhat more complicated. Nevertheless, we can still do a good job as long as the chargino decay has a sufficient Q value.

As a case very different from the example given in the preceding section, we study a chargino with a large Higgsino component in this section. The parameters we choose here are

$$m_0 = 400 \text{ GeV},$$
$$\mu = 250 \text{ GeV},$$
$$M_2 = 400 \text{ GeV},$$ (11)
$$\tan\beta = 2,$$

which give

$$\tilde{l}_R : 444.1 \text{ GeV},$$
$$\tilde{\chi}_1^\pm : 219.3 \text{ GeV},$$ (12)
$$\tilde{\chi}_1^0 : 169.2 \text{ GeV}.$$

In such a Higgsino-dominant case, the mass difference between the lighter chargino and the LSP is in general small ($\Delta m \simeq 50$ GeV $< m_W$ here), and the chargino decays mainly into a three-body final state to which the analysis in the preceding section does not apply at all.

We describe here our chargino selection at $\sqrt{s} = 500$ GeV in the Higgsino-dominant case. Although the best way to search for the Higgsino-dominant chargino is again to use the four-jet final state, we consider the lepton+two-jet mode for mass measurements: it is hard to select a jet pair resulting from a single chargino decay out of the four jets, since the jet pair now does not have any fixed invariant mass. Our selection criteria are (1) the number of tracks ≥ 5 which includes an energetic isolated e or μ ($E_l > 5$ GeV and the energy deposited by the other particles within the cone of a half-angle 30° around the lepton track is < 1 GeV), (2) 20 GeV $< E_{\text{vis}} < \sqrt{s} - 100$ GeV, (3) there are two jets for some $y_{\text{cut}} > 5 \times 10^{-3}$ with $m_{jj} < m_W - 12$ GeV and $E_{jj} < (\sqrt{s} - 100 \text{ GeV})/2$, (4) $|\cos\theta_j| < 0.9$, $|\cos\theta_l| < 0.9$, $-Q\cos\theta_l < 0.75$, $Q\cos\theta_{jj} < 0.75$, where Q is the lepton charge and θ_{jj} is the polar angle of the total momentum of the two-jet system, and (5) $|m_{l\nu} - m_W| > 10$ GeV for the W-pair hypothesis.

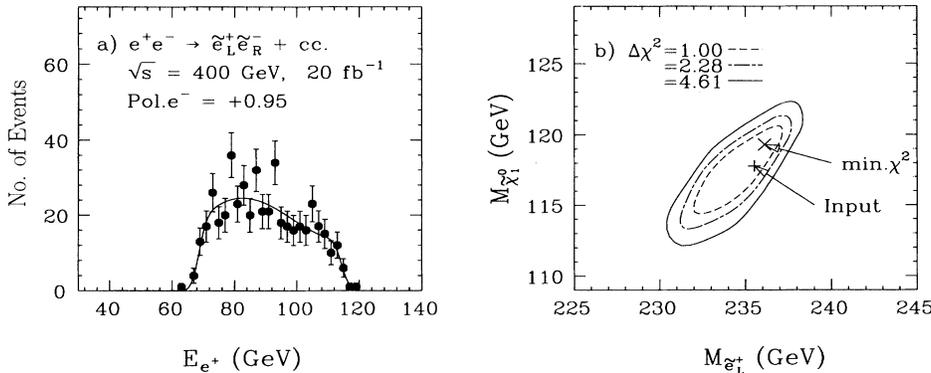Cuts 3–5 are to reduce the background from the W-pair and the $e^\pm \overset{(-)}{\nu}_e W^\mp$ productions [42]. Figure 21

a) $e^+e^- \to \tilde{e}_L^+\tilde{e}_R^- + $ cc.
$\sqrt{s} = 400$ GeV, 20 fb^{-1}
Pol.e$^-$ = +0.95

No. of Events

E_{e^+} (GeV)

b) $\Delta\chi^2 = 1.00$ ---
$= 2.28$ ----
$= 4.61$ ——

min.χ^2
Input

$M_{\tilde{\chi}_1^0}$ (GeV)

$M_{\tilde{e}_L^+}$ (GeV)

FIG. 18. (a) The energy distribution of final-state positrons for the candidate $\tilde{e}_L^\pm\tilde{e}_R^\mp$ events. The Monte Carlo data were generated at $\sqrt{s} = 400$ GeV for an integrated luminosity of 20 fb^{-1} and $P_{e^-} = +0.95$, after including the initial state radiation and the beamstrahlung effects. The smooth line is the best-fit curve from the two-parameter fit described in the text. (b) The contours from the two-parameter fit.

TABLE V. The observables in the slepton associate production.

$m_{\tilde{e}_L}, \sigma_R(\tilde{e}_R^-\tilde{e}_L^+), \sigma_L(\tilde{e}_L^-\tilde{e}_R^+)$, angular distributions

plots the acoplanarity angle between the lepton momentum and the total momentum of the two jets for the signal events (solid) and the background events from $e^+e^- \to W^+W^-$ (dash) and $e^{\pm} \overset{(-)}{\nu}_e W^{\mp}$ (dot), where an integrated luminosity of 20 fb^{-1} is assumed. It is clear from the figure that, when we apply an acoplanarity cut (6) $\theta_{\text{acop}} > 30°$, we can obtain a fairly pure event sample of the charginos. After this final cut, the detection efficiency is 10.3% and we obtain the total energy distribution of the two jets in Fig. 22(a), which gives us the mass of the chargino. A two-parameter fit to the distribution, varying the chargino and the LSP masses, yields the contours shown in Fig. 22(b). We can determine their masses with statistical accuracies of ±2.0 GeV and ±1.5 GeV, respectively, given an integrated luminosity of 20 fb^{-1}.

Once the masses and cross sections are measured, one can perform similar analyses as in the preceding section. One can determine $(M_2, \mu, \tan\beta)$ from the chargino mass, the LSP mass, and the total cross section from the right-handed electron beam, assuming the GUT-relation of the gaugino masses [43]. Then we can predict the masses of the second neutralino, the second chargino, etc., and can set the energy for the next threshold. If we do not discover them at the predicted masses, the SUSY-GUT with the minimal particle content is excluded. The angular distribution and the cross section for the left-handed electron beam give us the sneutrino mass, from which we obtain an upper bound on the left-handed slepton mass without any assumptions. By further assuming the universal scalar mass at the GUT scale $m_{\mathbf{5}^*} = m_{\mathbf{10}}$, we can also obtain an upper bound on the right-handed slepton mass. Then we can set the next target energy at the threshold of the right-handed slepton pair production. If we do not discover the right-handed slepton within the predicted mass range, the universal scalar mass assumption is violated (at least within the minimal particle content).

In this way, a systematic study on SUSY particles can be done for the lighter chargino case just as in the lighter slepton case.

B. Mixed region

The parameter sets, Eqs. (1) and (11), represent the cases where the light charginos and neutralinos are nearly pure gauginos or Higgsinos, respectively. Note that this is the generic situation for SUSY particles at linear collider energies, since there is substantial mixing only when
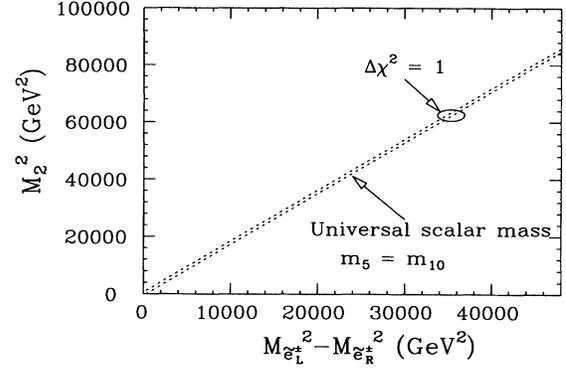

FIG. 19. The expected $\Delta\chi^2 = 1$ contour in the plane of the squared mass difference of the left-handed and the right-handed selectrons versus M_2^2. The dotted lines represent the universal scalar mass hypothesis for $\tan\beta = 0$ and 30.

$|M_2 - \mu| < m_W$ for charginos and $|M_i - \mu| < m_Z$ with $i = 1, 2$ for neutralinos. Note also that, even in the gaugino-dominant case, we had some sensitivity to μ, which, we believe, is a beautiful demonstration of the cleanness and precision of e^+e^- experiments.

It is, however, interesting to consider the case with substantial mixing, since this is the case where an e^+e^- collider with polarized beam proves most effective. Given a substantial Higgsino component in the lighter chargino, its pair production cross section is large enough to precisely measure the cross section and forward-backward asymmetry for a right-handed electron beam. The cross section and the asymmetry tell us both vector and axial-vector coupling constants to the U(1) gauge boson B, which in turn give us the two mixing angles of the chargino sector. Combined with the chargino mass measurement, we can determine all of the three parameters $(M_2, \mu, \tan\beta)$ in the chargino mass matrix. The mass of the neutralino in the chargino decay further constrains M_1, so that we can in principle measure all the four parameters, using only the first chargino pair production. This would be an interesting topic for future studies.

C. Complications

A complication occurs when several species of superparticles have nearly degenerate masses. Their thresholds open almost simultaneously, and it is in general hard to tell which event comes from which reaction. For example, some of the charginos and the neutralinos may be nearly mass degenerate and their signals overlap with each other. Even in such a case, energy scan, possible only at an e^+e^- collider, helps us sort out the signals:

TABLE VI. The physics implications of the observables in the slepton associate production.

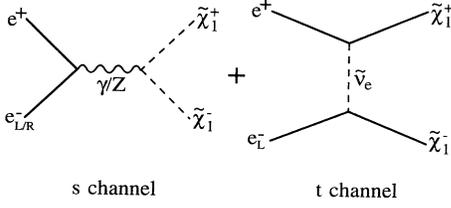|	
Universal scalar mass	$m_{\tilde{e}_R}, m_{\tilde{e}_R}, M_2$
Neutralino sector consistency	$\sigma_R(\tilde{e}_R^-\tilde{e}_L^+), \sigma_L(\tilde{e}_L^-\tilde{e}_R^+)$, angular distributions
Conservation of chirality	absence of $\sigma_R(\tilde{e}_L^-\tilde{e}_R^+), \sigma_L(\tilde{e}_R^-\tilde{e}_L^+)$

s channel   t channel

FIG. 20. Feynman diagrams for $e^+e^- \to \tilde{\chi}_1^+\tilde{\chi}_1^-$.

once some signals of new particles are found, we can carry out an energy scan in small steps to determine their thresholds. Another advantage of the e^+e^- collider is that any decay modes can be used to select the signal, while only those including some energetic lepton are useful at hadron colliders. One of such examples is already demonstrated in Sec. II. In our choice of parameters in Sec. II, we have both the $\tilde{\chi}_1^0\tilde{\chi}_2^0$ associate production and the $\tilde{e}_L\tilde{e}_R$ associate production at $\sqrt{s} = 400$ GeV. We could, however, resolve them, since $\tilde{e}_L$ decays only into an electron but $\tilde{\chi}_2^0$ has the muon mode as well. The thresholds for the $\tilde{\chi}_1^\pm$- and the $\tilde{\chi}_2^0$-pair productions were also close to each other. There, we have used the hadronic final state from $\tilde{\chi}_1^\pm \to \tilde{\chi}_1^0 W^\pm$, while $\tilde{\chi}_2^0$ only decays leptonically for our parameter set.

Heavier superparticles generally undergo cascade decays, which complicate the analyses. We emphasize again that e^+e^- colliders can gradually raise the center-of-mass energy so that the lightest one is discovered first, and its analysis is very simple as we demonstrated in the previous sections. By studying the first several superparticles precisely, we can determine all the masses below the next threshold. If we are lucky enough to reach the threshold of heavy ones, we can compare the observed complicated signatures with Monte Carlo generated events, using all the previously determined mass parameters. Dedicated studies are necessary to see whether we can sort out the signals. It is, however, worth recalling that the extremely
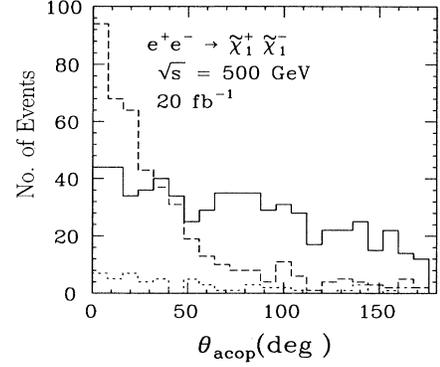

FIG. 21. The distribution of acoplanarity angles for the two-jet+lepton final states from the lighter chargino pair productions (solid) at $\sqrt{s} = 500$ GeV with initial state radiation and the beamstrahlung effects. The dashed and dotted histograms represent the background distributions expected for W^+W^- and $e^\pm \overset{(-)}{\nu}_e W^\mp$ productions, respectively.

complicated cascade decays discussed at hadron colliders [44] would not probably occur for the SUSY particles which are within the range of next-generation e^+e^- linear colliders.

When the decay of a superparticle has a very low Q value, its detection becomes very difficult. A typical example is the Higgsino-dominant chargino when $\mu \ll M_2$: the first chargino $\tilde{\chi}_1^\pm$ is nearly mass degenerate with the first and the second neutralinos, $\tilde{\chi}_1^0$ and $\tilde{\chi}_2^0$. The β decay of $\tilde{\chi}_1^\pm$ with a low Q value,

$$\tilde{\chi}_1^+ \to \tilde{\chi}_1^0 \nu_l l^+, \tilde{\chi}_1^0 q\bar{q}, \tag{13}$$

is hard to detect, even if its production cross section is large. The minimal detectable mass difference $\Delta m = m_{\tilde{\chi}_1^\pm} - m_{\tilde{\chi}_1^0}$ had been estimated to be 20 GeV in [16]. A similar problem also occurs when the right-handed slepton is nearly degenerate with B-ino-like neutralino, as in no-scale type initial condition $m_0 = 0$. It was estimated that one needs $m_{\tilde{l}} - m_{\tilde{\chi}_1^0} > 25$ GeV in Ref. [19]. We
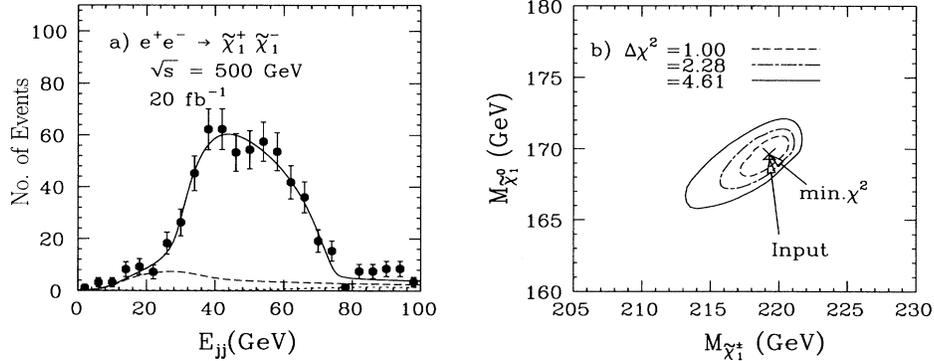

FIG. 22. (a) The energy distribution of the two-jet systems from the lighter chargino decays for Monte Carlo data generated at $\sqrt{s} = 500$ GeV with an integrated luminosity of 20 fb^{-1}, after including the initial state radiation and the beamstrahlung effects. The data points include both signal and background events. The solid line is the best-fit curve to the distribution, varying $m_{\tilde{\chi}_1^0}$ and $m_{\tilde{\chi}_1^\pm}$. The dashed and the dotted lines indicate, respectively, the expected shapes of the W^+W^- and the $e^\pm \overset{(-)}{\nu}_e W^\mp$ backgrounds. (b) The resultant contours from the two-parameter fit.

believe that this limitation can be relaxed considerably by using the right-handed electron beam which destroys most of the major background such as $e^+e^- \to W^+W^-$, while keeping a reasonable signal cross section. Apparently more work should be done on this point. Note also that the background from two-photon processes do not depend on the polarization while the signal does [45]. A dedicated study is necessary for this case, since the Higgsino-dominant neutralino or chargino may be the "first superparticle."

D. Limitations in mass measurements

Mass measurements using energy distributions of the decay products have been extremely useful in our study. A natural question is when and how this method breaks down.

Discoveries of sleptons and charginos are possible almost up to their kinematical limits at e^+e^- colliders. For instance, it was shown in Ref. [19] that it is possible to discover selectrons of mass 240 GeV at $\sqrt{s} = 500$ GeV, even though the cross section goes down as β^3. On the other hand, the studies we described in this paper obviously require sufficient statistics which are unavailable near the kinematical limits. We have to go well beyond the thresholds.

At the same time, we should not go too much above the thresholds. For instance, the lepton energies in slepton decays have a flat distribution in the range

$$\frac{m_{\tilde{l}}}{2}\left(1 - \frac{m_{\tilde{\chi}_1^0}^2}{m_{\tilde{l}}^2}\right)\gamma(1-\beta)$$

$$\leq E_l \leq \frac{m_{\tilde{l}}}{2}\left(1 - \frac{m_{\tilde{\chi}_1^0}^2}{m_{\tilde{l}}^2}\right)\gamma(1+\beta), \quad (14)$$

where

$$\gamma = \frac{\sqrt{s}}{2m_{\tilde{l}}}, \quad \beta = \sqrt{1 - \frac{4m_{\tilde{l}}^2}{s}}. \quad (15)$$

If β is too close to 1, the lower end point goes to 0 irrespective of the masses, so that we practically lose one of the two observables. The sensitivity to masses attains it maximum at a moderate value of $\beta \sim 0.5$.

Note that we can employ the virtue of linear colliders that the center-of-mass energy can be optimized flexibly to study each discovered superparticle.

We also extensively utilized the fact that the energy distributions of the decay products have relatively sharp edges. It is worth noting that complicated cascade decays do not spoil this property in general. For instance, let us take the case where the left-handed sleptons are lighter than the lighter charginos so that the decay $\tilde{\chi}_1^\pm \to l^\pm \tilde{\nu}_l$ or $\nu_l \tilde{l}_L^\pm$ is kinematically allowed. Then the decay is dominated by the cascade process $\tilde{\chi}_1^\pm \to l^\pm \tilde{\nu}_l$ or $\nu_l \tilde{l}_L^\pm$, followed by $\tilde{\nu}_l \to \nu_l \tilde{\chi}_1^0$ or $\tilde{l}_L^\pm \to l^\pm \tilde{\chi}_1^0$, so that there are always two invisible particles produced. The two branching ratios are almost the same when $m_{\tilde{l}_L}^2 \gg m_Z^2$. The lepton energy distribution is, therefore, the sum of a flat distribution coming from the direct decay $\tilde{\chi}_1^\pm \to l^\pm \tilde{\nu}_l$, and the convolution of two flat distributions from the cascade decay $\tilde{\chi}_1^\pm \to \tilde{l}^\pm \nu_l$ with $\tilde{l}^\pm \to l^\pm \tilde{\chi}_1^0$. The resultant energy distribution has a trapezoidal shape, still with relatively sharp edges. Furthermore, we already know, in this case, the masses of $\tilde{l}_L^\pm, \tilde{\chi}_1^0$, presumably $\tilde{\nu}_L^\pm$, combining the $\tilde{l}_L^\pm$ mass and $\tan\beta$ from Higgs sector. Then we can still measure $\tilde{\chi}_1^\pm$ mass quite well. If the decay goes directly into a three- (or more) body final state, the edges become less sharp. Recall that we faced this situation in a chargino decay (Sec. III A), where a 3% measurement of the chargino mass was still possible.

Truly annoying are those cascade decays which produce many invisible particles or those which leave only very small visible energies. For example, $\tilde{\chi}_i^0$ may decay mainly into $\tilde{\tau}^\pm \tau^\mp$, which might be the case for Higgsino-dominant one. There are too many parameters, in this case, to fit the observed energy spectrum and to extract the mass of the parent chargino. When the first chargino is a very pure Higgsino, then the mass difference from the lightest neutralino can be tiny. Then the visible energy is so small that one may not be able to discover it. Apparently more work should be done on these cases.

IV. CONCLUSION

We have carried out detailed Monte Carlo simulations of SUSY particle productions at a future linear e^+e^- collider for a typical choice of SUSY parameters. The simulations took into account realistic experimental conditions imposed by the machine and the detector threat. The results of the simulations demonstrated the effectiveness of the e^+e^- collider, which can be summarized as follows.

The e^+e^- machine provides not only an efficient way to discover supersymmetric particles but also a unique possibility of precision studies such as mass determinations and differential cross section measurements. For instance, the precision on mass measurement can be as good as 1% for leptonic final states and 3% for hadronic final states. It should be emphasized that this virtue of the e^+e^- collider crucially depends on its cleanness, well-defined initial state, and the availability of a highly polarized electron beam. In particular, the polarized electron beam will be an essential tool to control background and to sort our various components of a mass eigenstate. We have found that, from the first superparticle alone, we can learn a lot about the supersymmetry parameters, which guide us to the discovery of the next. This process will repeat itself until we exhaust all the superparticles kinematically accessible. More importantly, the parameter determinations through the measurements of the superparticle masses and cross sections enable us to test some key assumptions in supersymmetric grand unified models or supergravity, such as the gaugino mass relations and the universal scalar mass.

ACKNOWLEDGMENTS

APPENDIX A: BRIEF REVIEW OF SUPERPARTICLE MASS SPECTRUM

In this appendix, we briefly review properties of the minimal supersymmetric standard model (MSSM) used in this paper and discuss mass relations among superparticles.

We assume the minimal particle content of the supersymmetric standard model. We also assume that the lightest superparticle (LSP) is stable due to the R-parity conservation, or at least its lifetime is long enough so that it does not decay in a detector. Then signals of superparticles are associated with missing energies.

The superparticles are classified into the following sectors: neutralinos, charginos, sleptons, squarks, and gluinos. The neutralino sector in the MSSM consists of the two neutral gauginos $\tilde{B}$ (B-ino), $\tilde{W}^3$ (neutral W-ino), and the two neutral Higgsinos $\tilde{H}_1^0$, $\tilde{H}_2^0$, while the charged W-ino $\tilde{W}^\pm$ and the charged Higgsino $\tilde{H}^\pm$ constitute the chargino sector. The neutralinos, charginos, and sleptons are color singlet, and renormalization-group analyses imply that they are lighter than the others. This characteristic of the superparticle mass spectrum makes an e^+e^- collider a useful machine to search for the superparticles. The "first superparticle" in the e^+e^- collider will then be a slepton or a chargino. Occasionally a scalar top quark may be light and the first signal due to a large left-right

mixing in the mass matrix, but we disregard this possibility in this paper. In any case, the first superparticle decays into the LSP, which is usually assumed to be a neutralino.

Next we discuss the masses of the superparticles. For our present purposes, it is sufficient to consider those of the neutralinos, charginos, and sleptons. We will first explain the parameter set used in the Monte Carlo simulation. In the minimal supergravity, the soft SUSY-breaking parameters are only the following four: a universal scalar mass m_0, a universal gaugino mass $M_{1/2}$, a trilinear scalar coupling A, and B which appears in the Higgs mixing mass term. The slepton masses are parametrized by m_0 and $M_{1/2}$. In order to specify the neutralino and chargino sectors, we need additional two parameters: μ the supersymmetric Higgsino mass parameter and $\tan\beta$, the ratio of the vacuum expectation values of the two neutral Higgs scalars. The set of the four parameters [46]

$$m_0, M_{1/2}, \mu, \tan\beta \tag{A1}$$

completely specifies the mass spectrum and interactions of the superparticles we are now concerned with.

The gaugino mass parameters at the electroweak scale can be given by solving the renormalization-group equations. Under the assumptions of the minimal particle content and the universal gaugino mass at high energy scale, the gaugino mass parameters for the $U(1)_Y$ and $SU(2)_L$ are given by

$$M_1 = \frac{5}{3}\frac{\alpha'}{\alpha_U}M_{1/2} = 0.42M_{1/2}, \tag{A2}$$

$$M_2 = \frac{\alpha_2}{\alpha_U}M_{1/2} = 0.82M_{1/2}, \tag{A3}$$

respectively. Here α_U is the gauge coupling at the unification scale. Note that the mass relation

$$\frac{M_1}{M_2} = \frac{5}{3}\tan^2\theta_W = 0.50 \tag{A4}$$

holds for any GUT model at the one-loop level of the renormalization-group equations as long as the gauge group is unified into a simple group and the gaugino mass is universal at the GUT scale [47]. Therefore Eq. (A4) is called the GUT relation for the gaugino masses. The mass matrix of the neutralinos is written as

$$\begin{pmatrix} M_1 & 0 & -m_Z\sin\theta_W\cos\beta & m_Z\sin\theta_W\sin\beta \\ 0 & M_2 & m_Z\cos\theta_W\cos\beta & -m_Z\cos\theta_W\sin\beta \\ -m_Z\sin\theta_W\cos\beta & m_Z\cos\theta_W\cos\beta & 0 & -\mu \\ m_Z\sin\theta_W\sin\beta & -m_Z\cos\theta_W\sin\beta & -\mu & 0 \end{pmatrix}, \tag{A5}$$

on the $(\tilde{B}, \tilde{W}^3, \tilde{H}_1^0, \tilde{H}_2^0)$ basis. The mass eigenstates can be obtained by diagonalizing the mass matrix. The resulting mass eigenstates are denoted as $\tilde{\chi}_i^0$ ($i = 1, 2, 3, 4$) with masses $m_{\tilde{\chi}_1^0} < \cdots < m_{\tilde{\chi}_4^0}$. Similarly the chargino mass matrix is given as

$$\begin{pmatrix} M_2 & \sqrt{2}m_W\cos\beta \\ \sqrt{2}m_W\sin\beta & \mu \end{pmatrix}. \tag{A6}$$

We denote the lighter and the heavier charginos as $\tilde{\chi}_1^\pm$

and $\tilde{\chi}_2^\pm$, respectively.

The GUT relation for the gaugino masses was imposed in our Monte Carlo event generations and in many of our analyses. But we also showed that the global fit discussed in Sec. II C allows us to determine the masses of M_1 and M_2 independently and to test if Eq. (A4) is satisfied. If discrepancy with it is observed, the idea of the SUSY-GUT will run into serious trouble.

The slepton masses are also given as the solutions of the renormalization-group equations. In the minimal supergravity scenario, they are written in the form

$$m_{\tilde{l}_R}^2 = m_0^2 + 0.15 M_{1/2}^2 - \sin^2\theta_W m_Z^2 \cos2\beta, \qquad (A7)$$

$$m_{\tilde{l}_L}^2 = m_0^2 + 0.52 M_{1/2}^2 - \frac{1}{2}(1 - 2\sin^2\theta_W)m_Z^2\cos2\beta, \qquad (A8)$$

$$m_{\tilde{\nu}_L}^2 = m_0^2 + 0.52 M_{1/2}^2 + \frac{1}{2}m_Z^2\cos2\beta. \qquad (A9)$$

The first terms are boundary conditions at the GUT scale which are taken to be common under the assumption of the universal scalar mass, the second terms come from the renormalization-group effects, and the third ones are contributions from the D terms which arise at the electroweak symmetry breaking.

As was mentioned previously, we used the above formula of the slepton masses in the Monte Carlo simulation. If we relax the assumption of the universal scalar mass, the above relations will no longer hold. For example, in the SU(5) GUT with the minimal particle content below the GUT scale, we have

$$m_{\tilde{l}_R}^2 = m_{\mathbf{10}}^2 + 0.15 M_{1/2}^2 - \sin^2\theta_W m_Z^2 \cos2\beta - 0.053S, \qquad (A10)$$

$$m_{\tilde{l}_L}^2 = m_{\mathbf{5}^*}^2 + 0.52 M_{1/2}^2 - \frac{1}{2}(1 - 2\sin^2\theta_W)m_Z^2\cos2\beta \\ + 0.027S, \qquad (A11)$$

$$m_{\tilde{\nu}_L}^2 = m_{\mathbf{5}^*}^2 + 0.52 M_{1/2}^2 + \frac{1}{2}m_Z^2\cos2\beta + 0.027S, \quad (A12)$$

where S is defined by

$$S = m_2^2 - m_1^2 + \sum_{\text{generations}}(m_{\tilde{q}}^2 - 2m_{\tilde{u}}^2 + m_{\tilde{e}}^2 - m_{\tilde{l}}^2 + m_{\tilde{d}}^2), \qquad (A13)$$

which is evaluated at the GUT scale. Here m_1^2 and m_2^2 stand for the soft SUSY-breaking mass terms of the Higgs bosons with hypercharge $-\frac{1}{2}$ and $+\frac{1}{2}$, respectively. In the SU(5) GUT, it becomes simply

$$S = m_2^2 - m_1^2. \qquad (A14)$$

Note that S vanishes under the assumption of the universal scalar mass. From the SU(5) symmetry alone, $m_{\mathbf{10}}$

and $m_{\mathbf{5}^*}$ may be different. These could be even generation dependent. Note that, on the other hand, the mass difference of the doublet

$$m_{\tilde{l}_L}^2 - m_{\tilde{\nu}_L}^2 = -(1 - \sin^2\theta_W)m_Z^2\cos2\beta \qquad (A15)$$

is just the D-term contribution and is model independent.

The slepton mass relations can be used in a variety of ways. (a) In the SU(5) GUT, one can measure the difference

$$m_{\tilde{l}_L}^2 - m_{\tilde{l}_R}^2 = m_{\mathbf{5}^*}^2 - m_{\mathbf{10}}^2 + 0.37M_\infty^2 \\ - \frac{1}{2}(1 - 4\sin^2\theta_W)m_Z^2\cos2\beta + 0.080S, \qquad (A16)$$

and its dependence on β is extremely weak thanks to an accidental cancellation $1 - 4\sin^2\theta_W \simeq 0.07$. Assuming that the contribution from S is also negligible, a precise determination of left-handed and right-handed slepton masses measures the difference between $m_{\mathbf{10}}^2$ and $m_{\mathbf{5}^*}^2$. (b) Once we know $m_{\tilde{\nu}_L}^2$ from the t channel exchange in the chargino pair production, we can set an upper bound on the $m_{\tilde{l}_L}^2$ without assuming the GUT relation nor the minimal supergravity. (c) If we know $m_{\tilde{l}_R}^2$ and M_2 from the right-handed slepton and the chargino or neutralino studies, we can set an upper bound on $m_{\tilde{l}_L}^2$ assuming the universal scalar mass. Since the sensitivity to the t channel sneutrino exchange is weak for a Higgsino-dominant chargino, this may be also a useful tool to set the next target energy in this case.

APPENDIX B: MONTE CARLO SIMULATION

In our Monte Carlo simulations, we assumed the universal scalar mass at the GUT scale. Then the masses and the interactions of the neutralinos, the charginos, and the sleptons are parametrized by

$$m_0, M_2, \mu, \tan\beta. \qquad (B1)$$

We followed the convention of [48] in translating these parameters into particle masses and couplings. As for the standard model parameters, we have used $\alpha = 1/128$, $\sin^2\theta_W = 0.230$, $m_W = 80$ GeV, and $m_Z = 91.17$ GeV.

The Monte Carlo data used in this paper were generated as follows for both signal and background events. First we calculated, at the tree level, full helicity amplitudes including decays into final-state partons, using the HELAS library [49], which allows us to implement correct angular correlations and effects of the natural widths of unstable partons such as W and Z: our amplitudes for the background processes such as $e^+e^- \to e^\pm \overset{(-)}{\nu}_e W^\mp$, $e^+e^-W^+W^-$, etc. are thus exact, not based on the equivalent particle approximation. With this scheme, it is also easy to handle polarized beams.

The effective cross sections were then evaluated by the numerical integration package BASES/SPRING [50], taking into account the effects of initial state radiation, beam energy spread, and beamstrahlung [51]. We have used the

formula in [52] for the initial state radiation. The beam energy before beamstrahlung was assumed to have a flat distribution with a width of 1.0% in fullwidth at half maximum (FWHM) and that after the beamstrahlung was calculated by the formulas given in [53]. The input parameters to the formulas are the nominal beam energy (E^0), the number of particles in a single beam bunch (N), and the root-mean-square sizes of the beam (σ_x, σ_y, and σ_z). We have used $E^0 = 150$ GeV, $N = 0.63 \times 10^{10}$, $\sigma_x = 0.335$ μm, $\sigma_y = 0.00392$ μm, and $\sigma_z = 85$ μm for the simulations at $\sqrt{s} = 350$ and 400 GeV. For the simulations at $\sqrt{s} = 500$ GeV, we have switched the parameters to $E^0 = 250$ GeV, $N = 0.63 \times 10^{10}$, $\sigma_x = 0.260$ μm, $\sigma_y = 0.00304$ μm, and $\sigma_z = 67$ μm. These beam-related parameters were cited from [10].

The BASES/SPRING integration package enables us to generate four-momenta of final-state partons, once the integration is completed.

When these partons involved quarks, we used the LUND parton shower and string fragmentation programs [54]. The generated events were then processed through a detector simulator, in order to take into account the effects of the geometric acceptance and resolutions of our model detector described in [10]. The main detector components used in the analyses are the central drift chamber (CDC), the electromagnetic (EMC) and the hadron calorimeters (HDC), and the muon drift chamber. It should be noted that we tried to link charged particles detected in the CDC to energy clusters detected in the EMC or HDC, and, when linked, we used the CDC infor-

mation, since it has better resolution in general. To be realistic in this linking process, we generated calorimeter hits with a finite shower size and simulated the cluster overlapping.

The background processes included in our analyses are

$$e^+e^- \to W^+W^-, \tag{B2}$$

$$\to e^{\pm} \overset{(-)}{\nu}_e W^{\mp}, \tag{B3}$$

$$\to W^+W^-Z^0, \tag{B4}$$

$$\to e^+e^-W^+W^-, \tag{B5}$$

$$\to \nu_e\bar{\nu}_e W^+W^-, \tag{B6}$$

$$\to e^{\pm} \overset{(-)}{\nu}_e W^{\mp}Z^0. \tag{B7}$$

The other background processes

$$e^+e^- \to Z^0Z^0, \tag{B8}$$

$$\to e^+e^-Z^0, \tag{B9}$$

$$\to \nu_e\bar{\nu}_e Z^0, \tag{B10}$$

$$\to e^+e^-Z^0Z^0, \tag{B11}$$

$$\to \nu_e\bar{\nu}_e Z^0Z^0, \tag{B12}$$

$$\to \tau^+\tau^-, \tag{B13}$$

and two-photon processes were not simulated, but parton level calculations showed that they are completely negligible after the cuts described in the text. See also works by Grivaz [16] and Vander Velde [17]. The soft QCD backgrounds from initial state radiation and beamstrahlung photons were left out, since they are harmless according to the estimation in [10,55].

[1] M. Zolotarev, E. Kuraev, and V. Serbo, Inst. Yadernoi Fiziki Report No. 81-63 (unpublished); Report No. SLAC TRANS-227, 1987 (unpublished); P. Chen and V. Telnov, Phys. Rev. Lett. 63, 1796 (1989); T. Tauchi, K. Yokoya, and P. Chen, Particle Acc. 41, 29 (1993).

[2] M. Drees and R. Godbole, Z. Phys. C 59, 591 (1993).

[3] Proceedings of Workshop on Physics at Future Accelerators, La Thuile, Italy, 1987, edited by J. H. Mulvey (CERN Report No. 8707, Geneva, Switzerland, 1987).

[4] C. Ahn et al., "Opportunities and Requirements for Experimentation at a Very High-Energy e^+e^- Collider," Report No. SLAC-0329, 1989 (unpublished).

[5] Proceedings of the First JLC Workshop, Tsukuba, Japan, 1989, edited by S. Kawabata (KEK Report No. 90-2, Tsukuba, 1990).

[6] Proceedings of the Second JLC Workshop, Tsukuba, Japan, 1990, edited by S. Kawabata (KEK Report No. 91-10, Tsukuba, 1990).

[7] e^+e^- Collisions at 500 GeV: The Physical Potential, Proceedings of Workshop, Munich, Germany, Annecy, France, Hamburg, Germany, 1991, edited by P. M. Zerwas (DESY Report No. 92-123A/B, Hamburg, 1992).

[8] Proceedings of the Third JLC Workshop, Tsukuba, Japan, 1992, edited by A. Miyamoto (KEK Report No. 92-13, Tsukuba, 1990).

[9] Physics and Experiments with Linear Colliders, Proceedings of Workshop, Saariselkä, Finland, 1991, edited by R. Orava, P. Eerola, and M. Nordberg (World Scientific, Singapore, 1992).

[10] JLC Group, KEK Report No. 92-16, 1992 (unpublished).

[11] Proceedings of the Workshop on Physics and Experiments with Linear e^+e^- Colliders, Waikoloa, Hawaii, 1993, edited by F. Harris et al. (World Scientific, Singapore, 1993).

[12] Proceedings of European Meeting of the Working Groups on Physics and Experiments at Linear e^+e^- Colliders, Munich, Germany, Annecy, France, 1993, Hamburg, Germany, 1993, edited by P. M. Zerwas (DESY Report No. 93-123C, Hamburg).

[13] T. Maruyama et al., Phys. Rev. Lett. 66, 2351 (1991).

[14] T. Omori et al., Phys. Rev. Lett. 67, 3294 (1991); T. Nakanishi et al., Phys. Lett. A 158, 345 (1991); H. Aoyagi et al., ibid. 167, 415 (1992).

[15] ALEPH, DELPHI, L3, and OPAL, Phys. Lett. B 276, 247 (1992).

[16] J.-F. Grivaz, in e^+e^- Collisions at 500 MeV: The Physics Potential [7].

[17] C. Vander Velde, in e^+e^- Collisions at 500 MeV: The Physics Potential in [7].

[18] R. Becker and R. Starosta, in e^+e^- Collisions at 500 MeV: The Physics Potential [7].

[19] R. Becker and C. Vander Velde, in Proceedings of the Workshop on Physics and Experiments with Linear e^+e^- Colliders [11] and Proceedings of European Meeting of the Working Groups on Physics and Experiments at Linear e^+e^- Colliders [12].

[20] A. Bartl, W. Majerotto, and B. Mösslacher, in e^+e^- Collisions at 500 MeV: The Physics Potential [7].

[21] For review of supersymmetric models, see for example, H. E. Haber and G. L. Kane, Phys. Rep. **117**, 75 (1985). One can also find useful formulas for cross sections and decay rates at e^+e^- colliders, in H. Baer, A. Bartl, D. Karatas, W. Majerott, and X. Tata, Int. J. Mod. Phys. A **4**, 4111 (1989).

[22] See also L. J. Feng and D. E. Finnel, in *Proceedings of the Workshop on Physics and Experiments with Linear e^+e^- Colliders* [11] and Phys. Rev. D **49**, 2369 (1994), which discussed the squark mass determinations using polarized beam.

[23] K. Fujii, in *Proceedings of the ICEPP Symposium "From LEP to the Planck World,"* Tokyo, Japan, 1992, edited by K. Kawagoe and T. Kobayashi (UT-ICEPP Report No. 93-12, Tokyo, 1993), p. 157.

[24] T. Tsukamoto, in Proceedings of the Workshop on Physics and Experiments with Linear e^+e^- Colliders [11].

[25] In the previous reports, it was not systematically presented how the experiments would proceed. We have also redone the analyses including the following new points. (1) We now include more background processes as listed in Appendix B, while only harmful ones such as W^+W^- were included in Ref. [10]. The final figures do not show much difference, which in turn justifies our previous analyses. (2) The polarization of electron beam is now taken more realistically to be 95% instead of an ideal value of 100% in Ref. [24]. (3) We employ a better strategy for precision measurements: $m_{\tilde{e}_L}$ measurement in the associate $\tilde{e}_L^\pm \tilde{e}_R^\mp$ production instead of its pair production [10], and the use of acoplanar $\mu^+\mu^-$ final states to detect the associate $\tilde{\chi}_1^0 \tilde{\chi}_2^0$ production instead of e^+e^- final states [24] to avoid the "background" from $\tilde{e}_L^\pm \tilde{e}_R^\mp$. (4) We present completely new analyses: the associate $\tilde{e}_L^\pm \tilde{e}_R^\mp$ production and the chargino pair production in the case of two-body decay $\tilde{\chi}_1^\pm \to W^\pm \tilde{\chi}_1^0$.

[26] In Ref. [10], we ignored all the background processes but W^+W^- production, while in Ref. [24], we assumed 100% beam polarization. We now take into account other less serious background processes and a more realistic beam polarization of 95%.

[27] In the energy region of our interest, we can approximate Z to be massless and assume the $SU(2)_L \times U(1)_Y$ symmetry limit. In this limit, the $\tilde{e}_R$ pair production takes place via the annihilation into the $U(1)_Y$ gauge boson B. The signal cross section is thus enhanced, since right-handed electrons have a larger hypercharge than that of left-handed ones. On the other hand, the W^+W^- production is absent for the right-handed beam in the symmetry limit, since its s-channel diagram only involves the annihilation into the neutral $SU(2)_L$ gauge boson W^0 and its t-channel diagram has the exchange of the electron neutrino. As for the $e^\pm \overset{(-)}{\nu}_e W^\mp$ background, the right-handed electron eliminates diagrams with a t channel W exchange between the initial state e^+ and e^- which turned out to contribute dominantly after the angle cuts defined above.

[28] We have employed a cut on the acoplanarity angle instead of one on missing p_T, unlike in Refs. [16–19]. Their effects, are, however, essentially the same, resulting in comparable detection efficiencies.

[29] There are possibilities which invalidate the GUT relation of the gaugino masses even within the SUSY-GUT. First, the threshold corrections at the GUT scale may induce nonuniversal contributions to the three gaugino

masses [T. Goto, J. Hisano, and H. Murayama, Phys. Rev. D **49**, 1446 (1994)]. Second, the two-loop contribution to the renormalization group equations of gaugino masses destroy the universality [Y. Yamada, Phys. Lett. B **336**, 109 (1993); Phys. Rev. Lett. **72**, 25 (1994); S. Martin and M. Vaughn, Phys. Lett. B **318**, 331 (1993)]. These two effects are usually small, but may be large in special circumstances, for instance, when A or B is much larger than the gaugino mass. Finally, there may be higher dimension operators which break the universality. This contribution is suppressed by $M_{\rm GUT}/M_{\rm Planck}$, but may be large if the universal contribution is somehow small, or $M_{\rm GUT}$ is close to $M_{\rm Planck}$. It is an important question whether there are other possibilities to invalidate the GUT relation which we do not know at present.

[30] Since our parameter set gives a B-ino-dominant $\tilde{\chi}_1^0$ and a W-ino-dominant $\tilde{\chi}_2^0$, the left-handed electron beam is preferred from the view point of coupling strength. The left-handed electron beam, however, requires the t channel exchange of $\tilde{e}_L$ which is significantly heavier than $\tilde{e}_R$ here. Because of this propagator suppression and the smallness of hypercharge, the cross section for the left-handed electron beam is not very much different from that for the right-handed electron beam.

[31] In our preliminary study reported in Ref. [24], we used acoplanar e^+e^- final states.

[32] A. Miyamoto, in Proceedings of the Second JLC Workshop [6].

[33] This error is dominated by the statistical one. Note that 10% error is a pessimistic one because the $m_{\tilde{\nu}_e}$ in our parameter set happened to be at the minimum of the chargino production cross section (see Fig. 14). For other parameter sets (as in Sec. III A), the cross section is in general larger and hence the statistical error is smaller. Also, one can employ the right-handed electron beam to suppress background, when the chargino contains a substantial fraction of Higgsino state.

[34] We assumed here that we can determine the charge of at least one W candidate in a reconstructed event by using, for instance, the charge of a lepton from charm decay or the reconstruction of a charmed meson or both.

[35] The contours in Figs. 13(a)–13(c) are projections of the $\Delta\chi^2 = 1$, 2.28, and 4.61 hypersurfaces in the four-dimensional parameter space to two-dimensional subspaces. When the constant $\Delta\chi^2$ hypersurfaces are quadratic in the four-dimensional parameter space, their projections to a two-dimensional subspace become elliptic contours, corresponding to the confidence level values calculated with the χ^2 distribution for $N_{\rm DF} = 2$. The confidence level values obtained this way are 39%, 67%, and 90% for $\Delta\chi^2 = 1$, 2.28, and 4.61, respectively. As suggested by Figs. 13(b) and 13(c), however, the error hypersurfaces are far from ellipsoidal and the above confidence level values should not be taken literally.

[36] The cross section measurements of selectron and chargino pair productions are dominated by statistical errors in our case, as long as we know luminosity and beam polarization with accuracies better than 1%.

[37] The ambiguities in μ and $\tan\beta$ slightly enlarge the errors on M_1 and M_2. This is why the use of a 95% polarized electron beam made the M_1-M_2 contour slightly larger than that in Ref. [24], where 100% was assumed.

[38] Note that this upper bound is obtained without assuming boundary conditions at the GUT or Planck scales. It

can be derived solely from the weak-scale supersymmetric Lagrangian.

[39] This center-of-mass energy is actually lower than the chargino-pair threshold, which is specific to our choice of parameters. The associate $\tilde{e}_L \tilde{e}_R$ production should have been already observed when we studied associate $\tilde{\chi}_1^0 \tilde{\chi}_2^0$ production in Sec. II B. Though the cross section for $\tilde{\chi}_1^0 \tilde{\chi}_2^0$ is much lower than $\tilde{e}_L \tilde{e}_R$, the signals of these two processes can be separated since $\tilde{e}_L$ decays only into an electron while $\tilde{\chi}_2^0$ has both $e^= E^- \tilde{\chi}_1^0$ and $\mu^+ \mu^- \tilde{\chi}_1^0$ modes.

[40] There may be overlaps in the scatter plot between the $\tilde{e}_R$-pair and the $\tilde{e}_R \tilde{e}_L$ associate productions for a different combination of masses. Then a useful observable is the asymmetry of the events with $E_{e^-} > E_{e^+}$ and $E_{e^+} > E_{e^-}$. Once the asymmetry is found, we can extract $m_{\tilde{e}_L}$ from the electron and the positron energy distributions, since we already know $m_{\tilde{e}_R}$ and $m_{\tilde{\chi}_1^0}$.

[41] It is an interesting possibility to check the radiative breaking scenario (K. Inoue, A. Kakuto, H. Komatsu, and S. Takeshita, Prog. Theor. Phys. **68**, 927 (1982); L. Ibanez and G. Ross, Phys. Lett. **110B**, 215 (1982); L. Alvarez-Gaumé, J. Polchinski, and M. Wise, Nucl. Phys. **B221**, 495 (1983). This requires a detailed study of the Higgs sector, including both light and heavy ones.

[42] We assumed here that the two-body mode has been searched for and not found, which justifies the application of the mass cut to eliminate W's.

[43] If we know $\tan\beta$ from the Higgs sector, then we can further vary M_1 and M_2 independently to test the GUT relation at this stage.

[44] For example, see, H. Baer, C. Kao, and X. Tata, Phys.

Rev. D **48**, 2978 (1993).

[45] M. Drees (private communication).

[46] In Sec. II we used the $SU(2)_L$ gaugino mass parameter M_2 instead of $M_{1/2}$. The relation between these two is given by the renormalization-group equations [see Eq. (A3)].

[47] Y. Kawamura, H. Murayama, and M. Yamaguchi, Phys. Lett. B **324**, 52 (1994).

[48] K. Hikasa, JLC SUSY Manual (unpublished).

[49] H. Murayama, I. Watanabe, and K. Hagiwara, KEK Report No. 91-11, 1992 (unpublished).

[50] S. Kawabata, Comput. Phys. Comm. **41**, 127 (1986).

[51] We did not include the initial state radiation and the beam effects for the background from the fusion processes: $e^+e^- \rightarrow e^+e^- W^+W^-$, $e^{\pm}\nu_e^{(-)}W^{\mp}Z^0$, and $\nu_e\bar{\nu}_e W^+W^-$. Since both the initial state radiation and the beam effects make the cross sections for these processes smaller, our background estimation is conservative.

[52] F. Berends, *Z Physics at LEP I*, Proceeding of the Workshop, Geneva, Switzerland, 1989, edited by G. Altarelli, R. Kleiss, and C. Verzegnassi (CERN Yellow Report No. 89-08, Geneva, 1989), Vol. 1.

[53] K. Yokoya, Proceedings of 1988 Linear Accelerator Conference, CEBAF Report No. 89-001, 1989 (unpublished), p. 494.

[54] T. Sjöstrand and M. Bengtsson, Comput. Phys. Comm. **43**, 367 (1987).

[55] P. Chen, T. L. Barklow, and M. E. Peskin, Phys. Rev. D **49**, 3209 (1994).